TU Delft

Delft University of Technology

Document Version
Final published version

Licence
CC BY

Citation (APA)
Terrazas Villarroel, L. G., Wenninger, J., Heredia-Gómez, M., van de Giesen, N., & McClain, M. E. (2026). Monitoring Oxbow Lakes with Remote Sensing: Insights into Turbidity, Connectivity, and Fish Habitat. *Remote Sensing*, *18*(3), Article 474. https://doi.org/10.3390/rs18030474

Important note
To cite this publication, please use the final published version (if applicable).
Please check the document version above.

Copyright
In case the licence states “Dutch Copyright Act (Article 25fa)”, this publication was made available Green Open Access via the TU Delft Institutional Repository pursuant to Dutch Copyright Act (Article 25fa, the Taverne amendment). This provision does not affect copyright ownership.
Unless copyright is transferred by contract or statute, it remains with the copyright holder.

Sharing and reuse
Other than for strictly personal use, it is not permitted to download, forward or distribute the text or part of it, without the consent of the author(s) and/or copyright holder(s), unless the work is under an open content license such as Creative Commons.

Takedown policy
Please contact us and provide details if you believe this document breaches copyrights.
We will remove access to the work immediately and investigate your claim.

This work is downloaded from Delft University of Technology.

remote sensing

MDPI

Article

Monitoring Oxbow Lakes with Remote Sensing: Insights into Turbidity, Connectivity, and Fish Habitat

Lina G. Terrazas-Villarroel [1,2,*], Jochen Wenninger [1], Marcelo Heredia-Gómez [3], Nick van de Giesen [2] and Michael E. McClain [1,2]

[1] Department of Water Resources and Ecosystems, IHE Delft Institute for Water Education, Westvest 7, 2611 AX Delft, The Netherlands; j.wenninger@un-ihe.org (J.W.); m.mcclain@un-ihe.org (M.E.M.)
[2] Department of Water Management, Delft University of Technology, Stevinweg 1, 2628 CN Delft, The Netherlands; n.c.vandegiesen@tudelft.nl
[3] Laboratorio de Hidráulica, Universidad Mayor de San Simón, Petrolera Ave. Km 4.2, Tamborada Zone, Torres Sofer, Cochabamba 6760, Bolivia; m.heredia@umss.edu
* Correspondence: l.g.terrazasvillarroel@tudelft.nl or linaterrazas@gmail.com

Highlights

What are the main findings?

- Multitemporal surface reflectance shows trends in oxbow lake area and water types.
- Oxbow lake connectivity peaks during the flooding period under natural conditions.

What are the implications of the main findings?

- Connectivity-based groups of oxbow lakes represent the availability of fish habitat.
- Oxbow lake diversity and connectivity are essential for river ecological integrity.

Abstract

In meandering river floodplain systems, remote sensing is a valuable tool for assessing connectivity processes relevant to fish ecological functions. This study used the Google Earth Engine platform and multispectral Landsat 7 imagery. A random forest classifier was used to evaluate water types and area changes in oxbow lakes of the Beni River in Bolivia. Water type dynamics were mainly associated with lake age and distance from the main channel. Seasonal variations highlighted the role of wind-driven sediment resuspension and overflow during high discharge conditions. Long-term lake area changes reflected typical oxbow lake evolution as well as alterations caused by the main channel. Multiannual changes showed a notable area decrease during years of low discharge. Relationships between discharge and lake area dynamics allowed the classification of three lake groups with different levels of connectivity and overbank flow influence. The ecological relevance of these groups was evaluated based on fish habitat preferences and migration patterns. Results emphasize the importance of preserving natural hydrologic variability, with flooding associated with increased habitat availability. Overall, this study demonstrates the usefulness of satellite remote sensing for detecting ecohydrological processes and offers insights to preserve ecological functions in data-scarce regions.

Keywords: meandering river; oxbow lakes; remote sensing; Google Earth Engine; ecohydrology

Check for updates

Academic Editor: Zhijun Li and Lilong Zou

Received: 17 December 2025
Revised: 23 January 2026
Accepted: 25 January 2026
Published: 2 February 2026

Copyright: © 2026 by the authors. Licensee MDPI, Basel, Switzerland. This article is an open access article distributed under the terms and conditions of the Creative Commons Attribution (CC BY) license.

1. Introduction

In large river floodplains where the main channel carries substantial sediment loads, water surface reflectance represents water quality and connectivity processes relevant to

ecological functions [1–3]. Water turbidity associated with suspended sediment reflects key characteristics linked to fish habitat preferences [4]. In addition, hydrologic connectivity among water bodies is vital for aquatic habitat availability [5,6]. Long-term satellite records and platforms such as Google Earth Engine help characterize water surface reflectance, turbidity, and flooded area over time and space [7–9]. Analyzing these dynamics provides insights into habitat characteristics, while understanding their relationship with hydrologic variability helps evaluate the potential impact of hydrologic alterations.

In river floodplain systems, surface hydrologic connectivity among water bodies determines their status as lentic or lotic aquatic habitats [10]. In systems where overbank flow is the primary driver of connectivity, its ecological influence is described by the flood pulse concept [6]. Fish rely on this connectivity to access habitats and complete their life cycles. They migrate to floodplains for spawning, feeding, and shelter during extended and predictable flood pulses. As water levels recede, fish return to the main channel or tributaries [11–13]. Fish abundance is essential to riverine communities that rely on this resource for their livelihoods. High recruitment and growth rates are often linked to extreme flooding events and flooded areas, leading to higher catches in subsequent years [14,15]. Seasonal flood pulse variability affects fish concentration and fishing effort, with higher catches during low flow periods and lower catches during floods as fish disperse into inaccessible floodplains [16,17].

Meandering channels are the most common pattern in systems where the main channel dominates connectivity [10,18,19]. Their aquatic habitat structure includes the main channel, oxbow lakes, connection channels, and internal drainages. The formation of cutoffs and oxbow lakes is influenced by slope, vegetation density, and bank erodibility [20]. Following cutoffs, oxbow lakes evolve through typical life stages, from initial plug bar formation to progressive sedimentary infilling and eventual near-complete infill [21,22]. Lake responses to flood pulses have been linked to characteristics such as lake age, orientation angle, and distance from the main channel [23–25]. To evaluate connectivity, previous studies have integrated oxbow lake life stages with the flood pulse concept, emphasizing functional differences among these stages [24].

Seasonal changes in water turbidity, driven by suspended sediment, also influence fish habitat preferences and behavior. Reduced light availability affects fish sensory responses, altering predator–prey interactions and modifying prey abundance [4,26]. In addition, water bodies with higher turbidity have been associated with a greater presence of detritivorous fish species [27].

Water turbidity in meandering rivers can be represented by surface reflectance, especially in rivers with high sediment loads [2,3,28]. Relationships between water optical properties and physico-chemical parameters have been widely used to classify water types in different regions [29,30]. Optical water types identified in Brazilian waters reflect dominant limnological traits associated with turbidity, trophic status, and organic matter [31,32]. An increase in suspended particles is often linked to the change in spectra in the green to near-infrared bands [33]. In turn, sediment settling enhances light penetration and photosynthetic activity, increasing chlorophyll levels. Together, these optical responses provide proxies that reflect sediment dynamics and hydrologic conditions in river floodplain environments.

Remote sensing has become a key tool for monitoring river floodplain waters due to its spatiotemporal coverage of optical properties. Several studies have characterized channel-floodplain dynamics by monitoring water type transitions that reveal areas of dilution, sedimentation, flow reversal, backwater effects, and wind-driven resuspension [2,33–37]. The classification of water types is often performed using machine learning methods [38]. Among these, the widely used random forest classifier consists of an ensemble of decision

trees that introduce randomness in their building process [39]. These classifiers have been used to assess hydrologic connectivity in floodplain lakes, classify land cover and water areas in wetlands, and distinguish water types based on water quality parameters [25,37]. A key advantage of decision tree classifiers is their flexibility in handling different feature subsets and decision rules, balancing accuracy and efficiency [40]. Random forest classifiers also allow the estimation of feature importance while maintaining high predictive performance [37].

Previous studies in the Amazon basin have assessed hydrologic connectivity of oxbow lakes using optical image classification [25,41]. However, reliance on high-resolution commercial imagery limits transferability and long-term analysis. A recent study in the Beni River evaluated oxbow lake hydrologic dynamics using remotely sensed area changes and rainfall patterns [42], but did not incorporate river discharge data or water optical proxies that are particularly relevant in turbid systems. Field-based studies in other regions have provided insights into physico-chemical processes within individual oxbow lakes [24,43]; however, their specificity and cost limit their application to multi-lake assessments. In this paper, we address these limitations by applying a multitemporal, satellite-based analysis that combines lake area dynamics, water optical types, and river hydrologic variability to infer hydrologic connectivity and habitat availability in a turbid river floodplain system. This approach enables a comparative, long-term assessment of oxbow lake dynamics and their ecological relevance in a low-data region.

2. Materials and Methods

2.1. Case Study

The meandering Beni River originates in the Eastern Andes and flows 840 km through Bolivia's lowlands to its confluence with the Madre de Dios River (see location in Figure 1a). This study covers a 250 km reach downstream of the town of Rurrenabaque, which is the primary fish landing site concentrating small-scale production (see Figure 1b). Our focus is on key fishing locations within this reach, including the main channel and forty oxbow lakes, as indicated by local fishers [44].

The climate in the region presents a seasonally distinct pattern, with the rainy season from November to March and the dry period from April to October. Significant moisture flux from the Atlantic and Amazon rainforest is retained by Andean orography, creating rainfall hotspots in various locations [45]. The discharge at Rurrenabaque station presents a typical southern tropical unimodal regime with mean monthly discharges ranging from 760 m^3/s in August to 4700 m^3/s in February. Also, the interannual variability is high, with frequent peaks and low flows [46]. Several floods were linked to La Niña events, and no long-term negative trend was observed during the wet season. Additionally, there is an intensification of the dry period associated with changes in rainfall timing. The mean monthly wind speed varies from 4.2 km/h in June to 8.3 km/h in September, remaining above 7.5 km/h until December.

The Beni River is notable for its high sediment load, with an estimated mean suspended sediment load of 200 million tons/year (+/−27%) at the Rurrenabaque station [47]. This high sediment transport has been correlated to high meandering and cutoff rates within the Amazon River network [48]. The primary factors influencing main channel migration are the heterogeneity of the banks, with clay-rich zones acting as hinge points and sandy banks migrating actively [49]. An evaluation of the influence of hydrology on meandering dynamics used topographic data and satellite images to estimate erosion and deposition rates, revealing links with the intensity, timing, and duration of bankfull flow [50]. This study also described the behavior of oxbow lakes based on their age and changes in flooded area, emphasizing the role of the connection channel and its capacity to allow flood inflow

and return flows. Sediment deposition in the oxbow lakes varied with the distance from the main channel and the connectivity angle. Field measurements in one oxbow lake revealed sediment variation linked to overflow duration, local rain influence, local erosion, and wind-driven sediment resuspension [23].

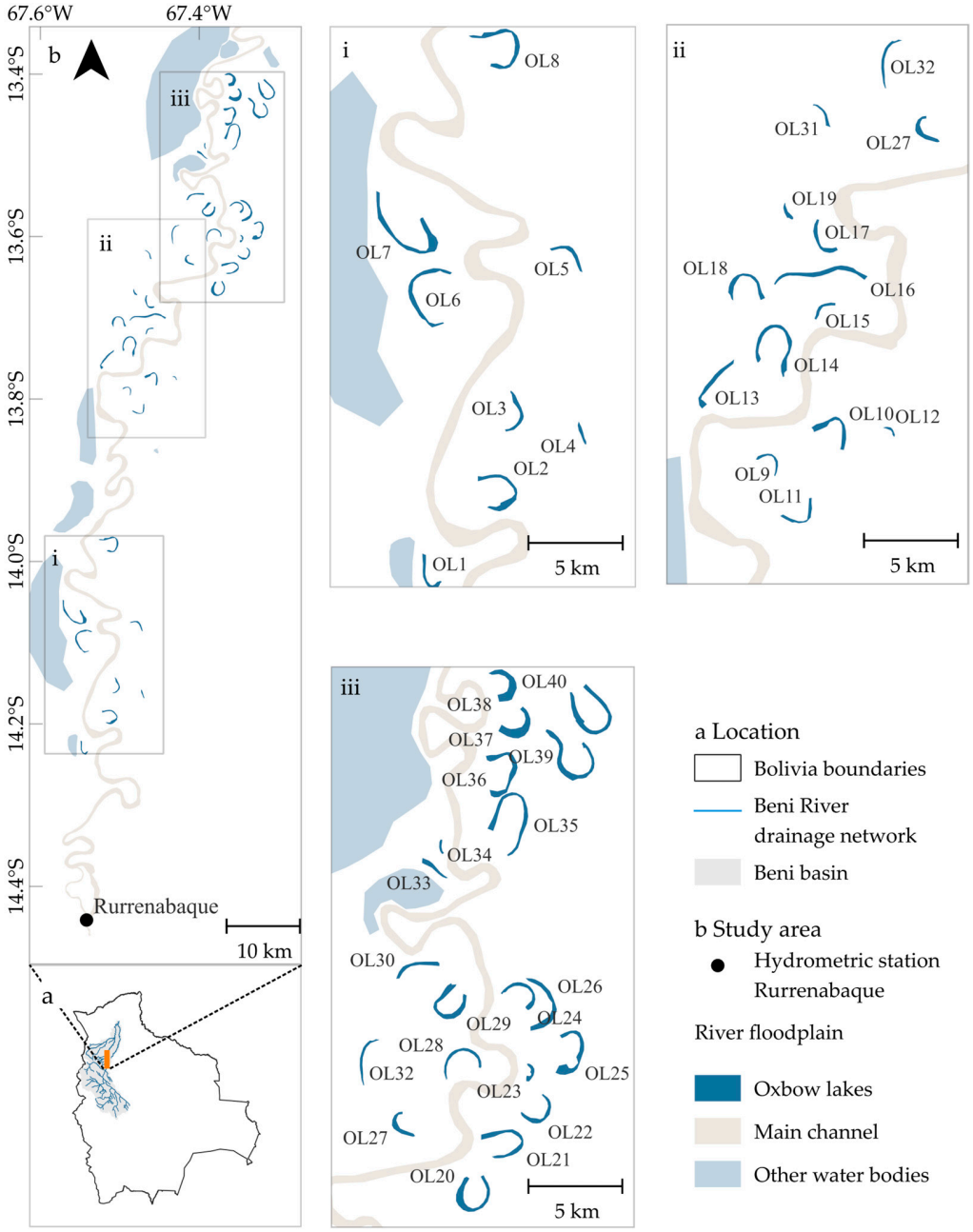

Figure 1. (**a**) Location of study area; (**b**) study reach of the Beni River indicating the location of the hydrometric station Rurrenabaque, oxbow lakes, and water bodies detailed in areas (**i**–**iii**).

The Beni River floodplain system plays a vital role as an aquatic habitat for fish that support the livelihoods of small-scale riverine communities. The influence of hydrology on this ecological function and socioeconomic activity was explored through local fishers' knowledge [44]. Fishers highlight the importance of water body connectivity, flood duration, and extent. They use this information to predict future catches, select fishing locations, and plan trips, similar to other fishers in the region [14–17]. In addition, the fishers associated fish species with habitat characteristics such as turbidity.

2.2. Available Data

The selection of the satellite data sensor was based on its suitability to represent the Beni River system. The Landsat 7 Enhanced Thematic Mapper plus (ETM+) sensor was selected because it acquires satellite images with 6 reflective bands, 30 m spatial resolution, 15-day revisit frequency, and data available from 1999 until 2023. This period is the longest compared to Landsat 5, Landsat 8, and Sentinel 2. The data were accessed through the Google Earth Engine (GEE) catalog, specifically Level 2, Collection 2, Tier 1, courtesy of the U.S. Geological Survey (Reston, VA, USA). This dataset contains ready-to-use atmospherically corrected surface reflectance created using the Landsat Ecosystem Disturbance Adaptive Processing System (LEDAPS) algorithm [51]. Additionally, images accessed through Google Earth Pro's (version 7.3.6.10441) timeline were used to visually analyze patterns at higher spatial resolution.

Image filtering and preprocessing were performed in GEE, applying first a 40% cloud coverage threshold to the entire image and later a 20% limit within each oxbow lake polygon to mask clouds. Thus, the number of images varies among lakes, especially when local or sparse clouds only affect a group of lakes. Then, for each lake, the calculated area (after land cover classification) was screened for values outside the 10th and 90th percentiles. These images were inspected for residual clouds, haze, or cloud shadows and removed from the analysis of that lake. The monthly distribution of valid satellite images per each of the 40 lakes is indicated in Figure 2a. Finally, the areas in lakes affected by Scan Line Corrector-off (SLC-off) striping were corrected using a morphological mean filter applied to each band, with a square kernel of radius equal to 3 and 3 iterations. The number of affected lakes varies as the stripes originate farther or closer to the scene centerline; in the April 2022 image, half of the lakes were affected. Additional analysis of the stripe interpolation effect is presented in Appendix A. The resulting images were used for further analysis.

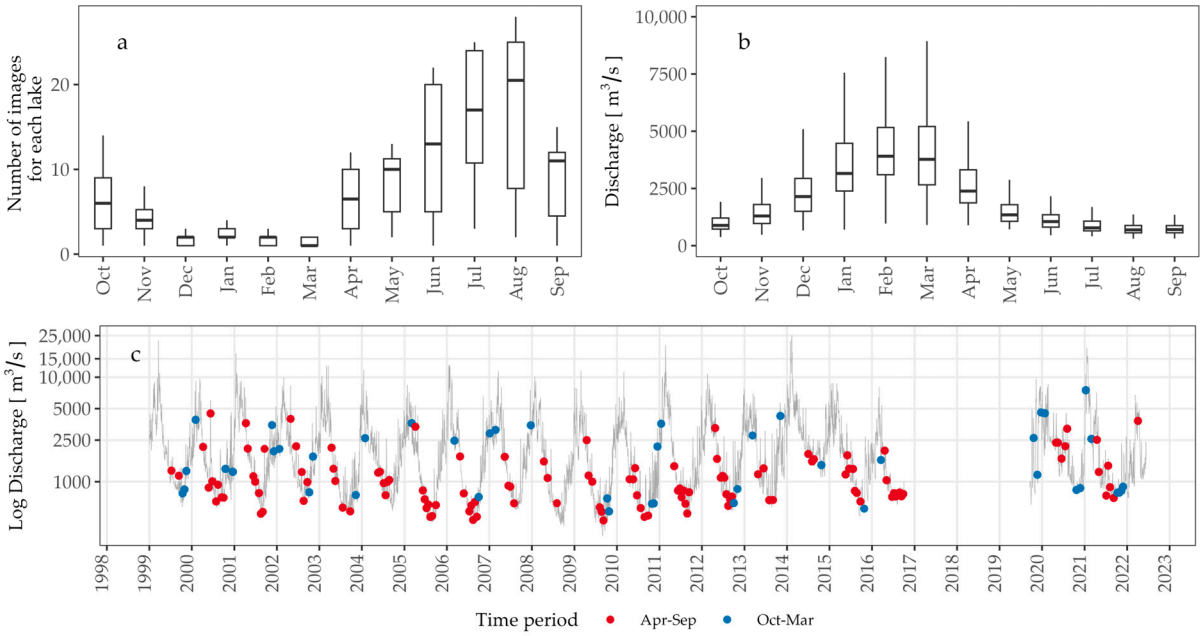

Figure 2. (**a**) Boxplot of image count per month per lake, (**b**) boxplot of monthly discharge [m^3/s] at Rurrenabaque, (**c**) daily discharge showing the timing of satellite images: red (April–September), blue (October–March).

Additionally, historical imagery from Google Earth Pro was used to identify lake formation years. Also, the analysis of wind-driven effects was performed using a high-

resolution image (©2020 Maxar Technologies, Westminster, CO, USA). Landsat 5 images corresponding to Level 2, Collection 2, Tier 1 were accessed through GEE (courtesy of the U.S. Geological Survey) and used to evaluate stripe interpolation effect. The hydrologic records at the Rurrenabaque station were accessed from Hydrologie et Géochimie du Bassin de l'Amazone (HyBAm) (https://hybam.obs-mip.fr/, accessed on 2 February 2022; note that the new platform may provide different access) and included observed water levels and calculated discharge values from 1989 to 2016. The analysis period was set to coincide with the availability of satellite images from 1999 onward. Water levels were not monitored from October 2016 to 2019, resulting in a data gap for this period. Water level measurements from October 2019 to October 2022 (provided by Servicio Nacional de Meteorologia e Hidrologia SENAMHI) were used to estimate discharge using adjusted rating curves [52]. Figure 2b presents the boxplot of monthly discharge at the Rurrenabaque station. The year was separated into two periods: October-March with low availability of satellite data and mainly wet conditions, and April-September with high availability of satellite data and primarily dry conditions. The hydrologic year was set to match these months. Figure 2c illustrates the daily hydrograph at Rurrenabaque station from 1999 to 2022, indicating the capture time of satellite images during these periods.

Wind speed data observed at the Rurrenabaque airport station was also recorded by SENAMHI. The period selected for analysis (2010–2016) follows a change in recording device and has continuous data.

2.3. Workflow and Conceptualization

Figure 3 presents the workflow of this study, indicating how remote sensing analysis of surface reflectance was used to inform habitat characteristics and availability for fish.

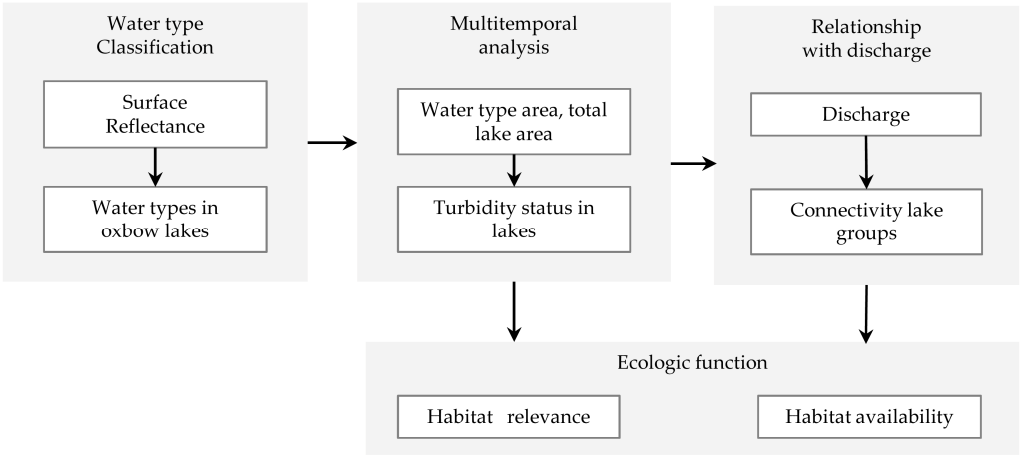

Figure 3. Workflow of analysis (detailed explanation of each step in Sections 2.4–2.7).

2.4. Classification of Water Types

The water type classification aims to distinguish turbid from non-turbid water in the oxbow lakes, which we interpret as reflecting changes in suspended sediment. The land cover and water types listed in Table 1 represent the dominant classes in the study area. We selected an image from the receding-water period (4 April 2022) because it contains a balanced combination of exposed sand, clear water, and turbid water, capturing spectral variability that is absent during peak flood or extreme dry conditions. Using an image with a broad set of spectral responses provides a robust basis for defining a representative classification scheme for oxbow lakes. Appendix B illustrates the spectral variability among oxbow lakes in this image and compares it with dry and flooded conditions.

Table 1. Spectral indices and thresholds to separate land and water types in 4 April 2022 image.

Type	Spectral Indices and Thresholds
Vegetation	$NDVI = \frac{NIR-Red}{NIR+Red}$, $NDVI > 0.6$ [50,51]
Exposed sand	$NSI = \frac{Green+Red}{\log SWIR1}$, $0.5 < NSI < 0.75$ [52]
Turbid water in main channel (WTO)	$0.1 < Red < 0.15$ and $0.1 < NIR < 0.15$
Very turbid water in oxbow lake (WTA)	$Red > 0.15$
Turbid water in oxbow lake (WTB)	$Green/Red < 1$
Water in oxbow lake with chlorophyll (WTC)	$Green/Red > 1$ [53]
Dark water in oxbow lake (WTD)	$Green < 0.05$

NDVI: Normalized Difference Vegetation Index, NSI: Normalized Sand Index; NIR: Near infrared, SWIR1: Short-wave infrared 1.

Class separation was guided by commonly used spectral indices. Vegetation was identified using the Normalized Difference Vegetation Index (NDVI) [53,54], exposed sand using the Normalized Sand Index (NSI) [55], and water bodies were first separated by hydromorphological setting (lotic main channel from lentic oxbow lakes). Water in the main channel showed stronger influence of the Near Infrared (NIR) band, while within oxbow lakes, a red-band gradient helped distinguish turbid from dark water. Intermediate water types were further separated using the green/red band ratio, which is sensitive to chlorophyll production [56] as light availability increases when sediment settles [36,57,58].

Figure 4 shows the mean surface reflectance values for each water type. The water types in oxbow lakes (WTA, WTB, WTC, and WTD) presented a gradual decrease in surface reflectance across all bands. WTO in the main channel indicated lower surface reflectance than WTA but resembled WTB in the blue and green bands while presenting higher values in the red and near-infrared.

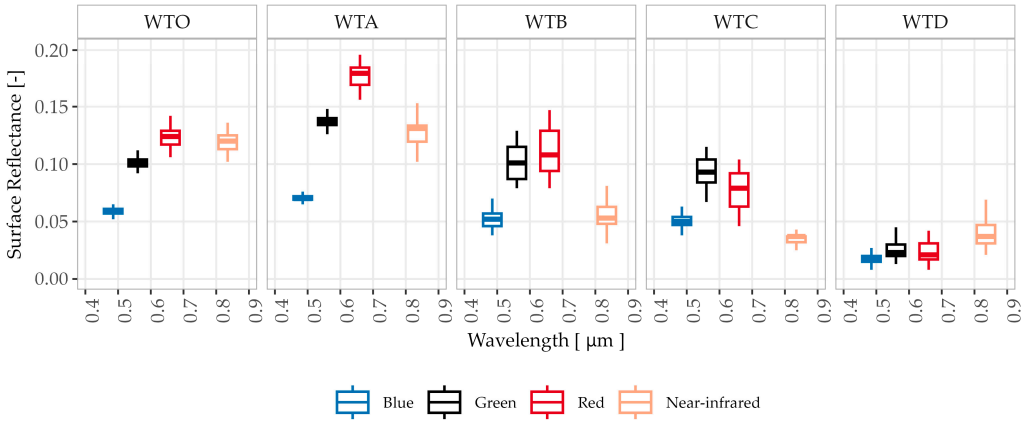

Figure 4. Mean surface reflectance of the water types in the blue, green, red, and near-infrared bands.

The classification was conducted in GEE using the Landsat 7 ETM+ image for 4 April 2022. For each class, an average of 208 points was identified as training and validation points. The training sample contained 65% of the points, while 35% were used for validation. A random forest algorithm was employed for the classification. This ensemble learning method is based on decision trees that incorporate randomness in their construction [38,39].

This process involves the random selection of training data subsets for each class and the definition of conditional rules using input variables, in this case, the surface reflectance of each band. These rules start with a root node and split into branches until they reach a leaf node, which represents the optimized probability of the sample belonging to the class. The parameters of the algorithm are the number of trees and the number of variables to consider at each split. They control the structure and randomness level of the forest. The

former was set to 50, and the latter was set to the square root of the number of variables. The prediction capacity of the random forest is the mean response from the regression trees. The internal classification consistency for the selected image was assessed with a confusion matrix and overall accuracy metrics. Additionally, the feature importance of each variable (surface reflectance in each band) was evaluated.

2.5. Multitemporal Analysis Approach

The classifier tree derived from the water type classification was applied to the pre-processed collection of images from 1999 to 2022. Afterwards, the area of each water type and total area were calculated for each oxbow lake throughout the analysis period. In order to allow for comparison among lakes, an area-weighted measure of turbid water types (turbidity status) was calculated for each lake as the percentage of the summed area of turbid water types (WTO, WTA, WTB) relative to the total water area of the lake. The turbidity status was separated into quartiles to categorize the dominant water type of each lake, with 0–24% representing low turbidity, 25–49% moderate low, 50–74% moderate high, and 75–100% high turbidity.

To compare the behavior of similar lakes, both qualitative and quantitative indicators were used to characterize them. Lakes that were modified as a result of the migration of the main channel into their area were identified, along with the year of alteration. Lake age was categorized into three groups based on the formation year identified through the historical imagery in Google Earth Pro: old (before 1999), middle-aged (1999–2013), and recent (after 2014). Dynamic characteristics, such as the distance from the closest plug bar to the continuously migrating main channel (along the direction of the connecting channel), were distinguished for the years 1999 and 2020 as close (<1300 m), medium (1300–2600 m), or far (>2600 m), and the change between those years as closer or farther. The recent lake area, calculated as the mean value over three years (2019–2022), was categorized into three size intervals: <1, 1–2, and >2 km^2. The relative frequency (%) of the turbidity status for each lake was aggregated over the study period, allowing lakes to be classified as primarily turbid lakes (frequency of low turbidity status lower than 33%), mainly clear lakes (dark and green, frequency of low turbidity status higher than 67%), or intermediate.

The multiannual analysis of lake area and turbidity status was divided into the two data periods described in Section 3.1. For the turbidity status, the most frequent status for each time step (month or year) was identified, and its relative frequency (%) was calculated across all lakes for the same time step. For the area analysis, the mean monthly difference (%) relative to the mean annual area was calculated for each lake and later averaged across all lakes. The annual area difference (%) was calculated relative to the recent area, and the variability was aggregated across all lakes. Finally, the dynamics of both variables in time, the timing of changes, and trends were associated with lake characteristics.

2.6. Evaluation of Relationship with Discharge

The relationship between discharge at the Rurrenabaque station and the variables in the oxbow lakes was evaluated through various steps. First, mean monthly and annual variability of discharge, lake area, and turbidity status were analyzed to identify multitemporal trends and relevant processes. Then, water types during an extreme hydrologic year were described to identify the causes of turbidity changes. For each lake, the relationship between area changes and discharge was evaluated in scatter plots, and similar patterns were used to group lakes. Finally, these patterns allowed an interpretation of the dominant hydrologic processes that cause area changes, and the identification of lakes in which overflow from the main channel is more relevant.

2.7. Interpretation of Ecological Functions

The availability and relevance of oxbow lakes as aquatic habitats were evaluated based on the aspects highlighted in the exploration of fishers' knowledge in [44]. Regarding fish habitat preference, fishers indicated that water clarity is associated with fish body cover, which also reflects the meat quality. The preferred scaled fish are commonly found in clear waters, in contrast to skin-covered fish that are mainly present in turbid waters.

Figure 5 presents fish migration patterns of native species and non-native *Arapaima gigas* (locally known as paiche). The year is divided into four periods: dry (July to October), rising waters (November to December), flooding (January to March), and receding waters (April to June). During the dry period, native fish species carry out their upstream reproduction migration along the main channel. As water levels rise, eggs drift, and juvenile fish migrate downstream, where connectivity from the main channel to the oxbow lakes allows them access to grow in these water bodies. During the flooding period, fish disperse into more distant oxbow lakes and flooded depressions. As water levels recede in the main channel, return flow from the oxbow to the main channel cues fish to begin their upstream migration again.

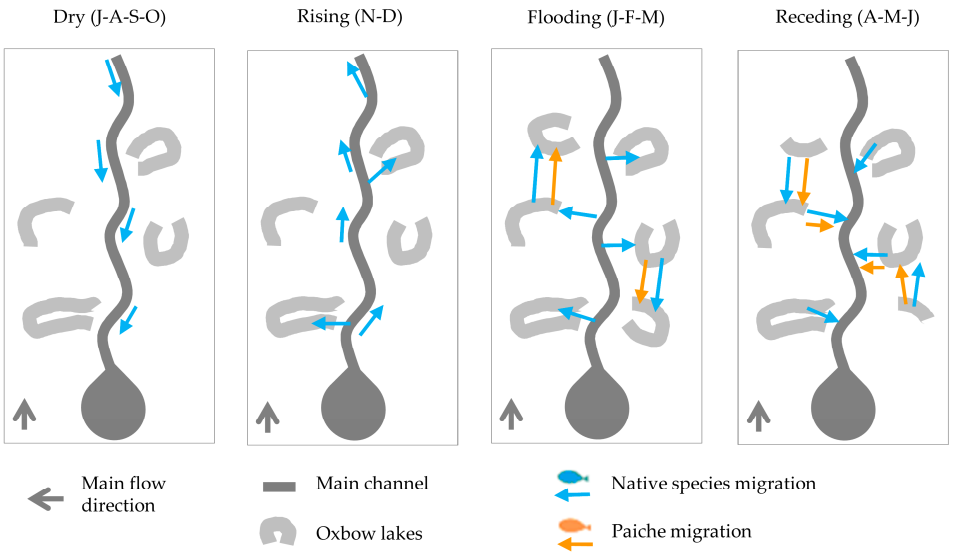

Figure 5. Conceptual model of Beni River connectivity and fish migration patterns of native species and the non-native paiche across hydrologic periods (adapted from [44]).

In contrast to the native fish species, the paiche primarily migrates between the main channel, oxbow lakes, and flooded depressions (bajíos) during the flooding and receding periods, completing most of its life stages in the oxbow lakes. For this species, the extent of flooding, both interannually and seasonally, is key to exploring new lakes, accessing food resources, and shelter in flooded depressions.

The selected satellite and hydrologic datasets allow the representation of physical habitat features that influence the ecological function of oxbow lakes. For instance, a seasonal increase in flooded area and shift to a turbid water type would reflect an increase in water input caused by overflow from the main channel (hydrologic connectivity), which enables fish access to oxbow lake habitats for refuge and food resources. In addition, the satellite-based classification of clear and turbid water types allows us to associate oxbow lakes and their most frequent water type with fish species based on their water type preferences. Furthermore, the water level variability in the main channel indicates periods of potential hydrologic connectivity or disconnection.

3. Results

3.1. Water Type Classification Results

Figure 6a presents the Landsat 7 ETM+ image (4 April 2022) in area iii, while Figure 6b shows the classified water types in each lake. Feature importance analysis identified near-infrared reflectance (31%) and the red band (20%) as the most relevant classification variables. The internal consistency check showed high agreement (99%) for the selected image, noting that both training and validation samples belong to the same date.

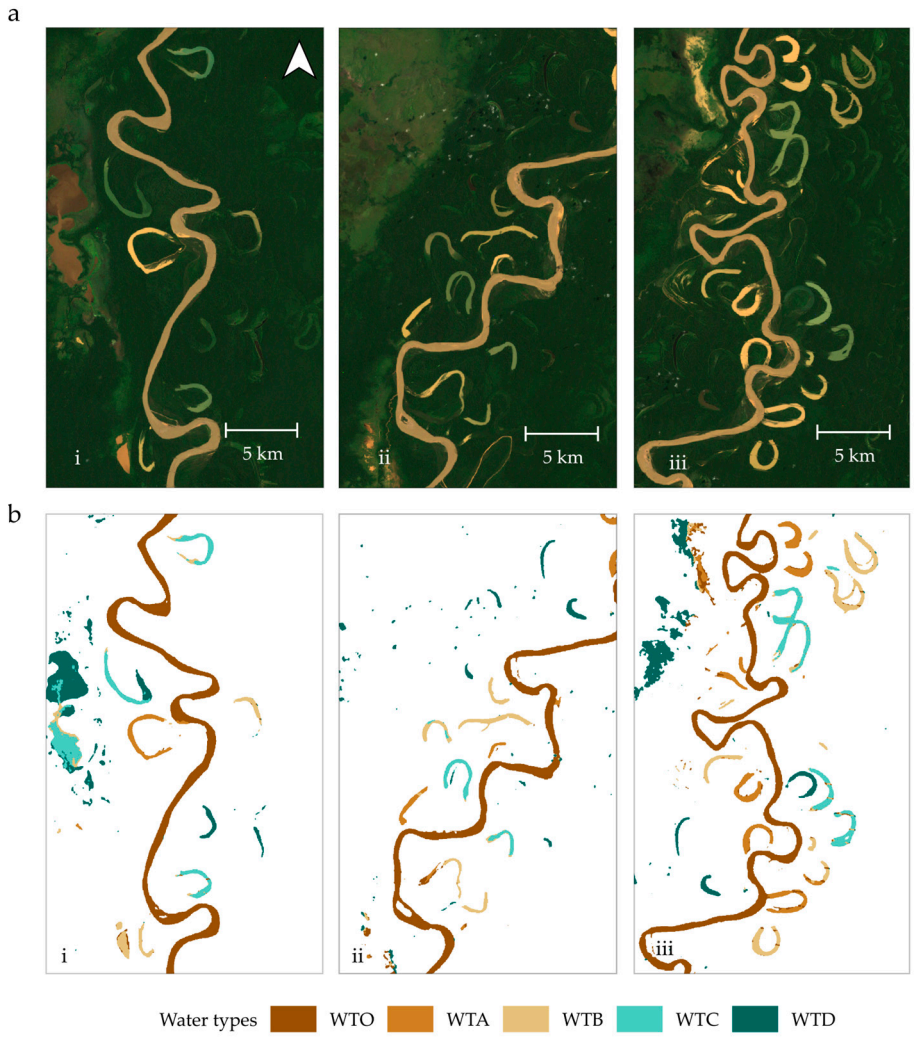

Figure 6. (**a**) Red, green, blue (RGB) composite of Landsat 7 ETM+ image of 4 April 2022 in areas (**i–iii**), and (**b**) classified image of water types in areas (**i–iii**).

3.2. Multitemporal Patterns of Lake Area and Water Types

Table A3 in Appendix C presents all lake properties, and Figure 7 illustrates important aspects: (a) satellite data availability (1999–2022), (b) mean recent lake area (2019–2022), and (c) turbidity status frequency % (1999–2022). Most oxbow lakes (23 of 40) were formed before 1999, with additional formations in 2001, 2005, 2008, and 2012–2018. Nine of these recently formed lakes were altered by main channel migration (AMC) into their area (2011 and 2019). Among the fifteen smallest lakes (<1 km^2), a few remained far from the main channel (6), while others suffered alterations (6). Nine lakes, mostly old (7) and distant from the main channel (2), presented a more frequent low turbidity status (clear). In contrast, ten lakes are primarily categorized as high turbidity (turbid), displaying formation or alteration post-2012 (6). No clear relationship exists between turbidity status and the recent lake area.

Figure 8a presents the most frequent monthly turbidity status for each lake. Low turbidity status is predominant in most lakes at the beginning of the dry period. This status is reached at different timings and persists for distinct months. Notably, 12 recently formed lakes (or altered) show late transition (June–July) and only 2 months of clear water status. The shift to intermediate turbidity status begins in August, September, and October for 15, 8, and 6 lakes. There are also four lakes (OL17, OL21, OL1, OL6) that consistently exhibit high turbidity year-round.

Figure 8b presents the annual turbidity frequency (%) across all lakes for the dry period (based on 101 valid images for at least 15 lakes compared to 18 images during the wet period). There were insufficient images for 1999, 2008, 2014, and 2022. Low turbidity prevailed (25–52% of images) in 2007, 2009–2010, 2013, and 2018. In contrast, high turbidity status was more common (25–30% of images) in 2000–2003, 2006, 2011, 2015–2016, and 2019–2021.

These multitemporal results indicate that turbidity dynamics are strongly seasonal and suggest a link to lake age and alteration with the main channel.

Figure 9a illustrates the mean monthly area difference (%) compared to the annual mean for each lake. Most lakes exceed the mean from January to July, showing mixed values during January-March due to limited satellite imagery. In contrast, a majority of lakes present small differences below the mean from August to December. Lake area variability is low, medium, and high for 21, 13, and 6 lakes (mainly turbid OL6, OL9, OL28, OL31, OL32, and OL33).

For multiannual trends, only dry-period data were used. Figure 9b presents the mean annual difference (%) relative to the recent area (2019–2022), indicating different trends: decreasing (positive difference for 11 lakes), increasing (negative difference for 5), mixed high variability (8), or stable (15). Eleven lakes decreased in area (notably OL5, OL12, OL13, and OL18), presenting old age (8) and medium to far distance to the main channel. In contrast, five lakes (OL1, OL16, OL33, OL35, and OL36) slightly expanded, displaying medium to high turbidity.

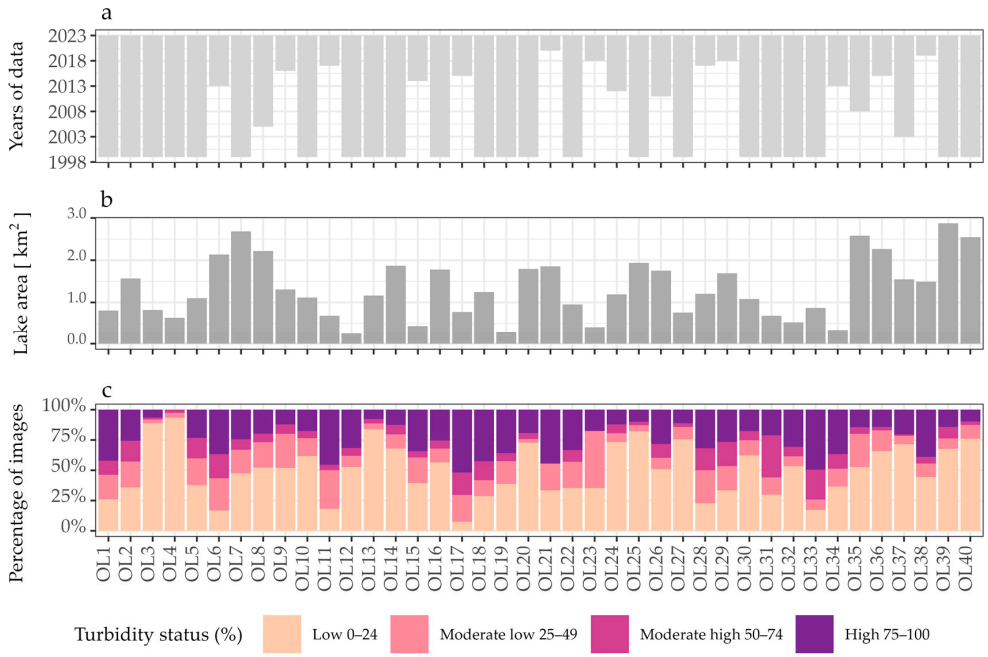

Figure 7. (**a**) Satellite data availability for each lake (1999 to 2022). (**b**) Mean recent lake area (2019–2022). (**c**) Turbidity status frequency (%) for each lake (1999 to 2022).

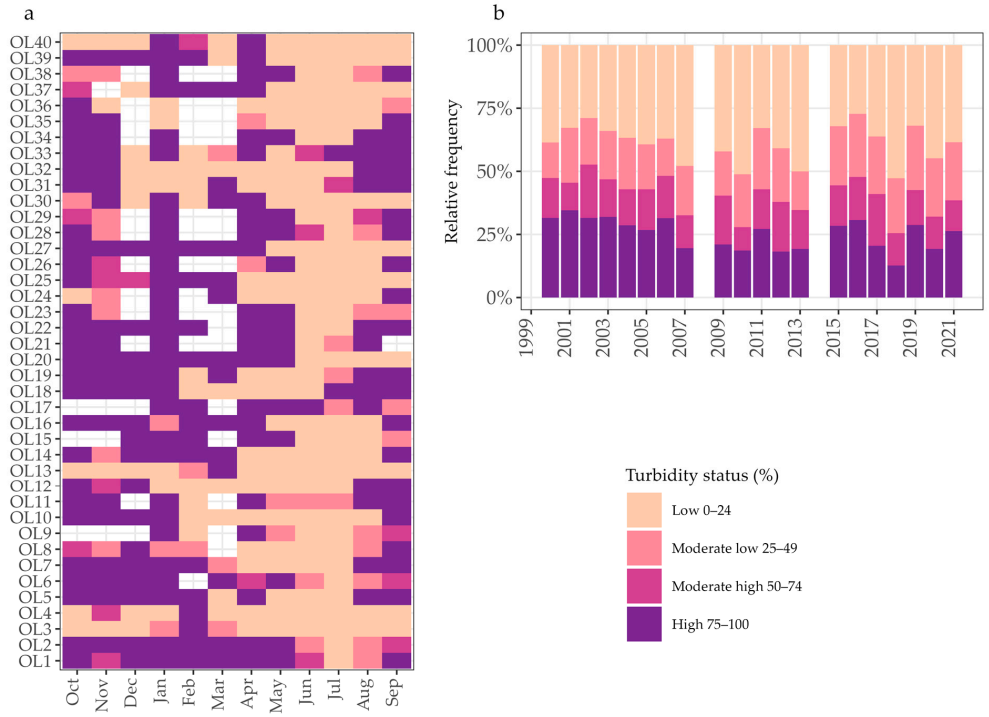

Figure 8. (**a**) Most frequent monthly turbidity status, and for the dry period (April–September); (**b**) multiannual turbidity status frequency (%) across all lakes.

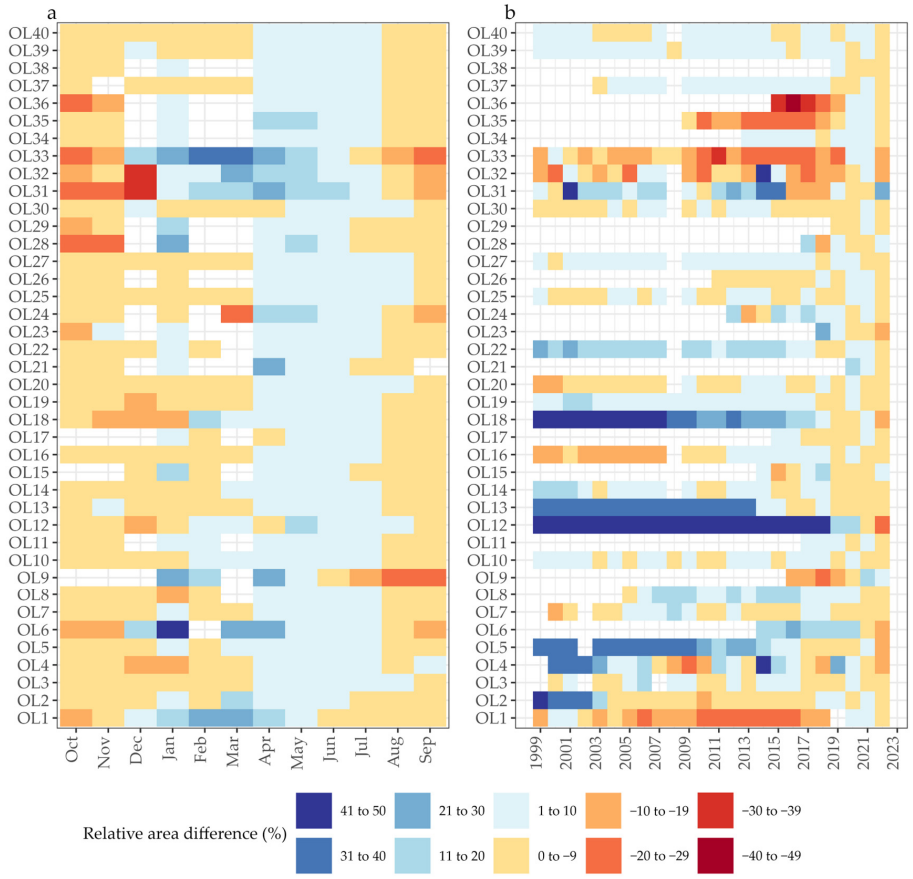

Figure 9. (**a**) Mean monthly area difference (%) compared to the annual mean, (**b**) mean annual difference (%) relative to the recent area (2019–2022).

3.3. Discharge Relationship with Lake Area and Water Types

The multitemporal comparison of discharge, lake area, and turbidity status is presented in Figure 10. The mean monthly lake area difference (Figure 10b) presents a break in February due to limited satellite imagery. The increase in lake area coincides with the rising discharge (Figure 10a) and remains above the mean until June, indicating the role of lakes as water storage. Figure 10c shows that low turbidity status frequency (%) peaks in June-July, but high turbidity status sharply increases in September and persists into the rising and flooding periods, despite the lake area continuously reducing until October.

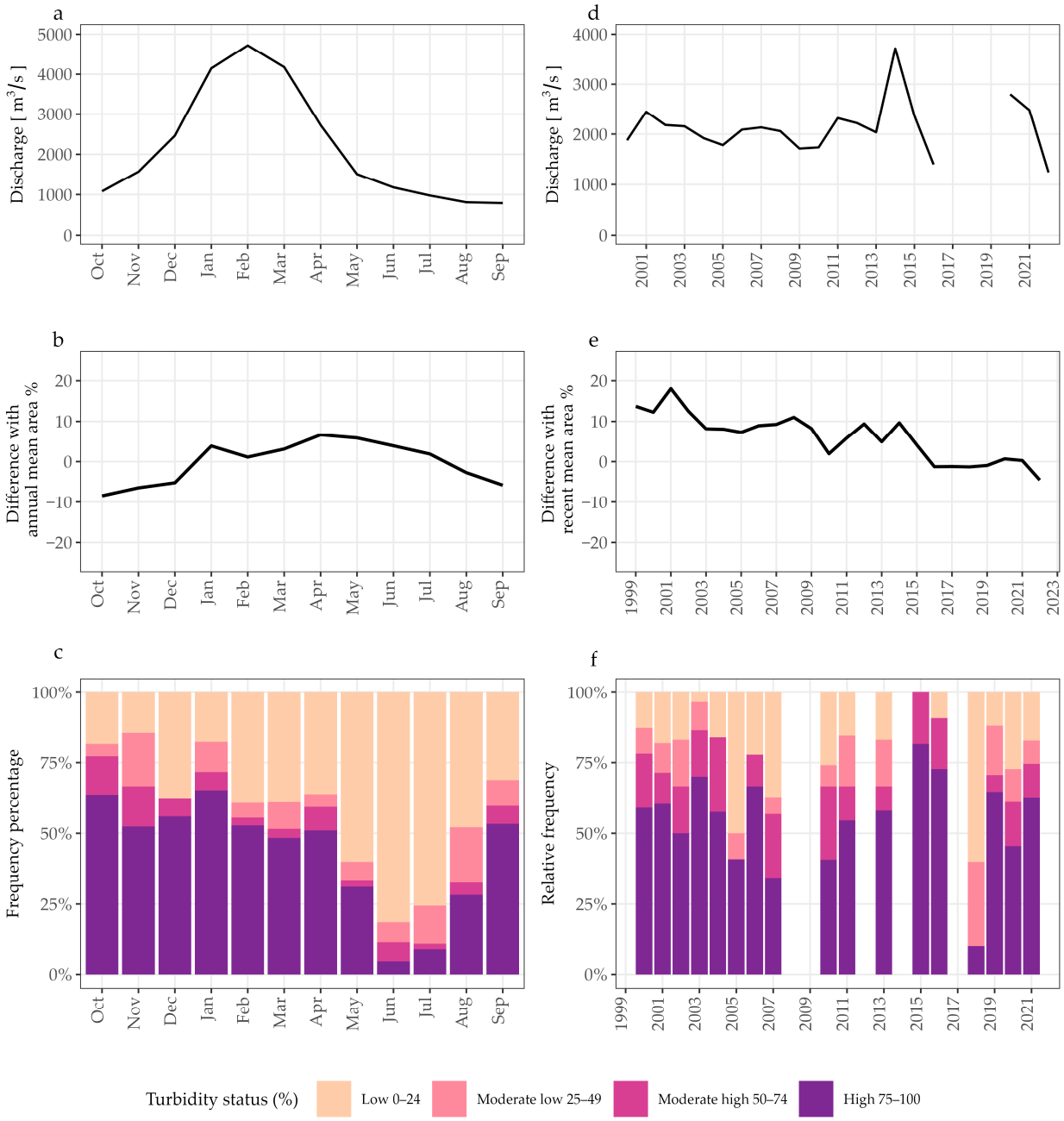

Figure 10. (**a**) Mean monthly discharge at Rurrenabaque. (**b**) Mean monthly area difference (%) with mean annual across all lakes. (**c**) Monthly turbidity status frequency (%) across all lakes. (**d**) Mean annual discharge at Rurrenabaque. (**e**) Mean annual difference (%) with recent area across all lakes. (**f**) Multiannual turbidity status frequency (%) across all lakes in the wet period (October–March).

Annual discharge variability (Figure 10d) is mainly coherent with mean annual lake area differences (%) with the recent area (Figure 10e, calculated with dry period data). Coincident lows occur in 2000, 2010, and 2016, while highs coincide in 2001 and the extreme year 2014. Figure 10f shows that annual turbidity status frequency (%) across all lakes is predominantly high during the wet period (45–75%), which considerably exceeds dry-period values (Figure 8b). Notably, high turbidity years include 2000, 2003, 2006, 2015–2016, 2019, and 2021, while lower values appear in 2005, 2010, and 2018, only coinciding with discharge lows in 2005 and 2010. This comparison is limited due to data gaps (2008–2009, 2014, and 2018) and the complex processes that affect lake behavior.

The transition of dominant water types was analyzed for the extreme hydrologic year 2020–2021. Figure 11a shows the hydrograph, indicating two satellite images: one during flooding (7500 m^3/s) and another at the end of the dry period (900 m^3/s). A middle-reach area was selected for analysis. Figure 11c illustrates the satellite and classified images, and Figure 11b displays the dominant water type per date and oxbow lake. During flooding, the dominant WTA indicates high turbidity associated with high discharge for all visible lakes. In contrast, at the end of the dry period, five lakes transition to clear WTC and dark WTD, while four lakes display turbid WTB, especially near the point bars.

Figure 11d illustrates a similar spatial variability in OL8 and OL29 using a high-resolution image from November 2020 (accessed from Google Earth Pro, ©2020 Maxar Technologies) and the corresponding satellite and classified images. The high-resolution image reveals a trace of suspended sediment originating at point bars, likely due to wind action; an extended evaluation of this driver is presented in Appendix D. These results emphasize the influence of wind at the beginning of rising waters and highlight the multiple drivers of turbidity dynamics in the oxbow lakes.

Figure 12 presents the relationship between discharge at Rurrenabaque (y-axis, logarithmic scale) and lake area difference from the annual mean (x-axis, %), with dot colors indicating dominant water types. Table A3 (Appendix C) presents the Pearson correlation coefficients for each lake and their statistical significance, assessed using a two-sided *t*-test (*p*-value and sample size). The correlation coefficients were used to categorize lakes into three groups:

- Group 1 (>0.4): fourteen lakes show a scattered log-linear increase (e.g., OL1, OL6, and OL33), with ten revealing a range of discharge values linked to the area above the mean. Most of these lakes (8) are recently formed, close to the main channel, and predominantly turbid;
- Group 2 (>0.1 and $\leq$0.4): thirteen lakes that exhibit a distinct separation of turbid and clear water types, corresponding to areas below and above the annual mean, respectively (e.g., OL10, OL22);
- Group 3 ($\leq$0.1): thirteen lakes predominantly older, clear water with minimal area changes (e.g., OL40) that have the least direct influence from main channel overflow.
- The categorization of recent lakes may change over time in response to river dynamics, particularly the migration of the main channel relative to lake position. Thus, the correlation analysis should be updated in future assessments.

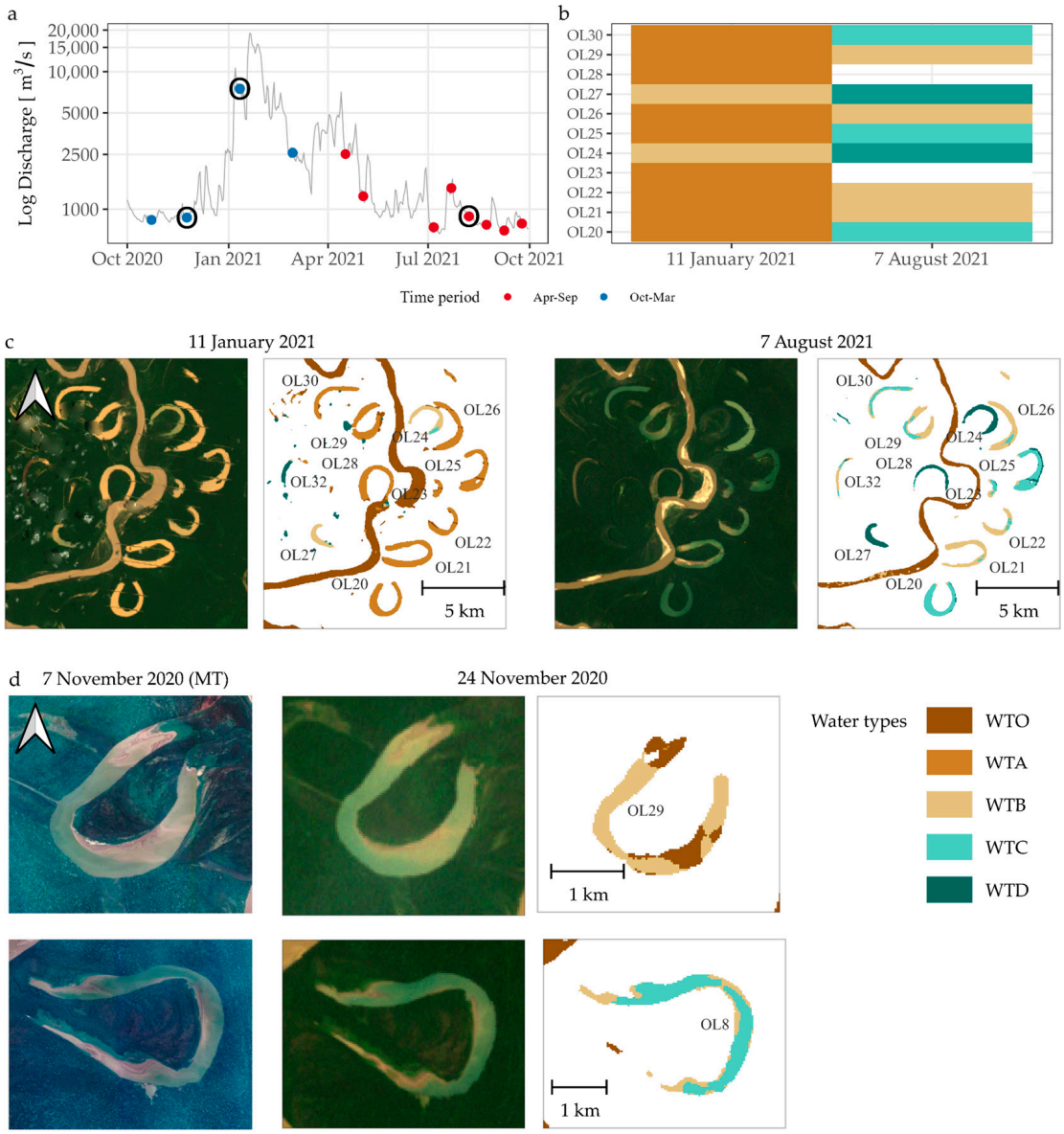

Figure 11. (**a**) Hydrograph for 2020–2021, indicating satellite images in wet and dry periods. For selected dates 11 January 2021 and 7 August 2021 (marked by the two rightmost black circles): (**b**) Tile plot of dominant water type in each lake, and (**c**) satellite (Landsat-7) and classified images. (**d**) High-resolution satellite image (accessed from Google Earth Pro, ©2020 Maxar Technologies) for 7 November 2020 and lakes OL29 and OL8, satellite (Landsat-7) and classified image for 24 November 2020 (indicated by the leftmost black circle).

3.4. Relevance of Oxbow Lakes as Fish Habitat

The relevance of oxbow lakes as fish habitat was evaluated based on characteristics in Table A3, Appendix C. The total lake area is 53 km^2, with 22% categorized as turbid—mainly recent oxbow lakes close to the main channel—associated with skin-covered fish (e.g., *Zungaro zungaro*), 56% intermediate, and 22% categorized as clear waters, mostly found in old lakes, which are more suitable for scaled fish species (e.g., *Pseudoplatystoma* spp.).

Habitat availability to fish species migrating from and to the river was derived from assumptions about surface hydrologic connectivity based on relationships between area changes, water type, and discharge. The total available habitat area of oxbow lakes is 49 km^2, distributed as 13.7 km^2 in Group 1 (28%), 15.2 km^2 in Group 2 (31%), and 20.1 km^2

in Group 3 (41%). Group 1 lakes display the highest correlation with discharge and have a direct influence on overflow during most of the year. In contrast, Group 3 lakes have the least frequent connectivity only during bankfull discharge, as evidenced by the changes in water type in Figure 11. Group 2 lakes represent an intermediate scenario in which the lack of discharge correlation and the presence of clear water, while exceeding the mean annual area, may indicate overflow with lower suspended sediment after settling along the connection channel. In addition, the occurrence of turbid water types below the mean area is associated with wind-driven resuspension during the dry and rising periods.

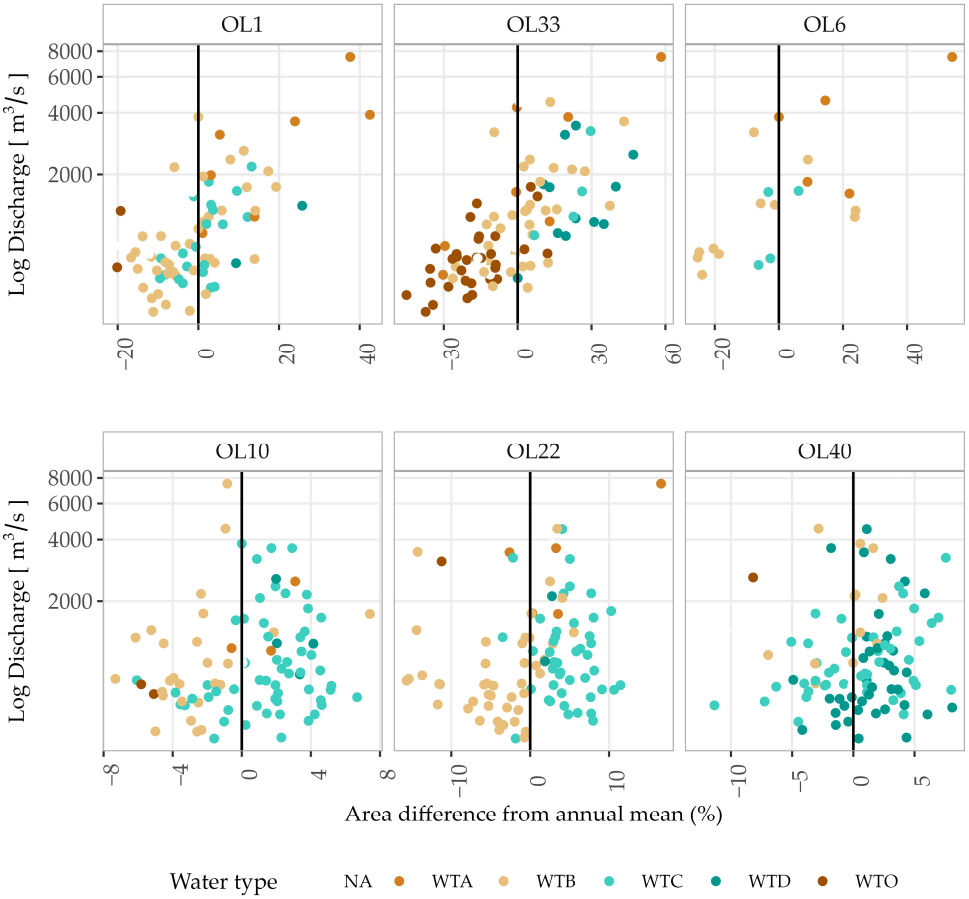

Figure 12. Scatter plot of area difference from annual mean (%) versus discharge (logarithmic scale), with dominant water type indicated by color for selected lakes. The black vertical lines indicate the zero value in the x axis.

For native fish species, Group 1 lakes are relevant, as early and late connectivity provide additional migration opportunities. For instance, juvenile species born early can access these habitats during the rising period, and species that reproduce late or undertake a second reproductive migration (e.g., *Prochilodus nigricans*) can access them during the receding period. For *Arapaima gigas*, which primarily inhabits oxbow lakes, Group 3 lakes serve as important refuges, as their primarily medium distance from the main channel reduces accessibility and minimizes the risk of alteration from channel migration, providing a more stable habitat.

In summary, the three lake groups reflect distinct patterns in area variability, water type trends, and relationship with discharge. These trends provide a quantitative basis to differentiate their hydrologic behavior and ecological function.

4. Discussion

The variability in surface reflectance among water types is consistent with regional classifications, with high relevance of red and near-infrared reflectance for turbid waters [29,59]. Higher surface reflectance of turbid water WTA compared to WTO results from higher scatter from finer sediment particles in the surface layer of the main channel that are transported to the lakes [60–62]. In addition, shallower depths of oxbow lakes compared to the main channel contribute to higher surface reflectance from the bottom [63].

Most oxbow lakes showed an intermediate turbidity (proxy) category, followed by clear and turbid, evenly distributed (Figure 7). Turbidity was mainly associated with lake age and distance from the main channel (Figure 8 and Table A3), similar to a previous study [64]. The analysis of discharge, lake area, turbidity status, and wind speed at the seasonal and event time-scale (Figures 10 and 11 and Appendix D) suggested that monthly turbidity changes were driven by hydrologic connectivity during the flooding period and by wind causing sediment resuspension in the dry period. Lakes with less frequent connectivity are likely to experience stronger wind-driven effects. The role of other processes, like rainfall erosion, requires further exploration [23].

Multiannual lake area changes primarily follow typical oxbow lake life stages (Figure 10), with sedimentation at point bars narrowing the inner bank and reducing the lake area [65]. These sedimentation rates depend on hydrologic connectivity and lake geometry, with frequent flooding and higher rates in the early stages [22,24] and lower rates as the main channel migrates away, which extends the connection channel and reduces its sediment conveyance efficiency until the lake area stabilizes [50,66,67]. These area trends are similar to recent regional observations [42]. A few lakes, however, experienced erosion due to main channel alteration (Figure 9 and Table A3). In these cases, overbank flow through the lake prevented sediment deposition and induced erosion, increasing the lake area.

Lake area changes are coherent with mean annual discharge trends (Figure 10), especially during low-flow years. Monthly lake area changes correlated well with discharge (Group 1) for recent lakes close to the main channel, while no correlation was found (Group 3) for older lakes located at a medium distance from the main channel (Figure 12). These patterns are coherent with previous studies evaluating relationships among lake age, distance from the main channel, and discharge [24,41]. For that reason, lake categorizations based on similar correlation analysis should be periodically reassessed as river dynamics evolve.

Hydrologic connectivity was represented by diverse processes and their interaction with lake properties, with turbidity changes highlighting notable sediment input during hydrologic events exceeding bankfull discharge (>6000 m^3/s [23] as shown in Figure 11). The influence of smaller events could be masked by wind-driven sediment resuspension. Monthly lake area and water type patterns suggest low-sediment water input likely causes hydrologic connectivity (Figure 12), potentially linked with lower discharge peaks, sediment settling along connection channels, or backwater effects. Additional water sources, such as rainfall, may extend connectivity duration [68]. The influence of each driver and flow direction depends on the hydrologic period. For instance, during the rising water period, a discharge threshold in the main channel is associated with connectivity, while during the receding period, thresholds of lake area or rainfall may represent connectivity to the main channel. Further studies are needed to improve our understanding of the interactions among these drivers, particularly for lakes in groups 2 and 3.

Oxbow lakes provide critical fish habitats, and turbidity categories reflect broader habitat conditions that may influence fish distribution [43,69]. In the study area, local fishers associated scaled fish with clear waters and skin-covered fish with turbid waters [44]. The habitat availability was assessed considering the connectivity-based lake groups, with

Group 1 lakes providing the highest duration, Group 3 lakes acting as key refuges, and Group 2 lakes as intermediate (Figure 12). Thus, these three lake groups serve as functionally distinct fish habitats with varied hydrologic connectivity, which highlights the complementary role of diverse oxbow lakes in supporting fish species with different life traits in the Beni River system. Other studies have evaluated the role of connectivity, turbidity levels, and lake characteristics as indicators of fish assemblages [70–72], highlighting higher fish richness associated with higher connectivity levels [73]. Further studies are needed to evaluate if these relationships are representative of the Beni River.

These ecohydrological insights can inform river management practices. The observed influence of hydrologic variability on habitat availability (through surface connectivity) highlights the importance of preserving natural flood dynamics in the river. These dependence links should be considered when evaluating potential hydrologic alterations, such as hydropower development. Flow regulation by dams typically dampens the seasonal hydrograph by reducing peak flows and increasing discharge in the dry period. These changes would lead to reduced flooded area and differentiated loss of oxbow lake habitats, as high (discharge) connectivity thresholds are no longer surpassed. Group 1 and 2 lakes, which rely on frequent and moderate connectivity, would experience fewer connectivity events. In contrast, Group 3 lakes that mainly connect during bankfull conditions would be vulnerable to permanent disconnection. These changes would block migratory routes of native species and diminish the extent of paiche habitat. Therefore, management strategies should incorporate connectivity thresholds of oxbow lakes to preserve hydrologic connectivity and mitigate habitat loss.

In general, habitat conservation strategies should ensure annual connectivity to all lakes and prevent lake infill in those with decreasing areas. Also, designating protected oxbow lakes based on species preferences can help maintain balanced trophic dynamics. Overall, the different turbidity and connectivity dynamics among oxbow lakes highlight their diversity and complexity as aquatic habitats for fish and their importance in preserving the ecological integrity of the river system.

Satellite data limitations include seasonal gaps during the flooding period (December–March), leading to underestimation of the frequency of turbid water types linked to hydrologic connectivity, as well as lower estimates of mean annual lake area and its correlation with discharge. In addition, the 15-day interval between satellite images hides short-duration events, resulting in missed short-term connectivity during the rising and receding periods. The 30 m resolution of Landsat 7 ETM+ also limits detection of narrow connection channels and fine-scale area changes, leading to underestimated lake area variability. Overall, these limitations produce conservative estimates of connectivity. Nevertheless, the main seasonal patterns and relative differences among lakes are expected to remain robust, as they are derived from multitemporal observations.

Analyses limitations of water type classification may mistype transitional pixels (such as wet sand during receding waters or dark vegetated water). Also, the discharge analysis omits flood wave travel and water mixing times (hours to days), which may result in satellite images capturing lagged hydrologic conditions. In addition, the interpretation of connectivity relying on the sediment-rich character of Andean–Amazon tributaries is site-specific. Therefore, relationships between turbidity proxies and connectivity may not transfer to clear-water systems or algae-dominated lakes. Lastly, the complex interaction of hydrologic connectivity drivers requires further evaluation through field validation.

Our study provides innovative insights into oxbow lake dynamics by integrating remote sensing and hydrologic data to assess connectivity, turbidity, and habitat availability. The integration of lake area and turbidity as indicators of hydrologic connectivity and their relevance to fish habitat offers a novel approach for evaluating aquatic ecosystems. The

study highlights the separation of processes driving turbidity changes, such as overbank flow and wind-driven sediment resuspension, which are often difficult to distinguish. In addition, the classification of lakes into connectivity-based groups (1, 2, and 3) provides a new framework for understanding their ecological roles, particularly in supporting fish migration and refuge habitats. The study also distinguishes the atypical behavior of oxbow lakes altered by a highly dynamic main channel, extending our knowledge of oxbow lake evolution. These findings contribute to conservation strategies by emphasizing the need for targeted habitat protection based on connectivity and turbidity dynamics, ensuring sustainable fish habitat and ecosystem integrity.

5. Conclusions

This study highlights the complex dynamics of oxbow lakes in the Beni River, as reflected by relationships among lake properties, hydrologic processes, and sediment-related proxies. Turbidity levels are associated with lake age, distance from the main channel, and inferred connectivity. These patterns are also consistent with wind-driven resuspension processes. Seasonal and long-term lake area changes reflect different patterns of lake evolution, influenced by differences in connectivity, sedimentation, and alteration by the main channel. The identified lake groups distinguish recent lakes near the main channel that experience frequent connectivity from older lakes that mainly connect during bankfull discharge. These ecohydrological insights suggest higher habitat availability during flooding conditions and highlight the importance of natural flooding dynamics. Overall, understanding the diversity of oxbow lakes dynamics provides valuable ecohydrological insights for river floodplain management and the preservation of ecological functions in these systems.

Author Contributions: Conceptualization, L.G.T.-V., J.W. and M.E.M.; Formal analysis, L.G.T.-V.; Funding acquisition, L.G.T.-V., M.H.-G., N.v.d.G. and M.E.M.; Methodology, L.G.T.-V.; Supervision, J.W., M.H.-G., N.v.d.G. and M.E.M.; Visualization, L.G.T.-V.; Writing—original draft, L.G.T.-V.; Writing—review and editing, J.W., M.H.-G., N.v.d.G. and M.E.M. All authors have read and agreed to the published version of the manuscript.

Funding: This work was supported by the Schlumberger Foundation's Faculty for the Future program and by the WWF Russell E. Train Education for Nature program (Grant number EF25156).

Data Availability Statement: The data that support the findings of this study are openly available in https://doi.org/10.5281/zenodo.15358712.

Conflicts of Interest: The authors declare no conflicts of interest.

Appendix A

We assessed the impact of Scan Line Corrector-off (SLC-off) striping on oxbow lake water area and turbidity-proxy estimates. Landsat 5 TM was used as an independent reference to Landsat 7 ETM+ because it provides similar spatial resolution, core spectral bands, and acquisition geometry. The Landsat 5 TM Level 2, Collection 2, Tier 1 imagery was obtained from the Google Earth Engine (GEE) catalog (courtesy of the U.S. Geological Survey).

To separate the effect of SLC-off stripes from expected spectral differences between sensors, lakes were separated into stripe-affected (intersecting SLC-off gaps) and unaffected. No cross-sensor harmonization or calibration adjustments were applied.

A low-cloud sequence in September 2009 included two consecutive Landsat 5 images (30 August and 15 September) and an intermediate Landsat 7 image (7 September). The median of the two Landsat 5 images and the single Landsat 7 image were preprocessed following the steps described in the main text. Then, the seven-type classification tree was applied to both images.

In 2009, 26 oxbow lakes existed; 18 were stripe-affected, and 8 were unaffected (see Figure A1b). For each lake, water area and turbidity proxy were calculated as indicated in Table A1, and group-level differences were summarized in Table A2.

For water area, unaffected lakes showed a mean difference between Landsat 5 and Landsat 7 of 0.4% (±2.3%), while affected lakes showed 2.5% (±3.2%). These marginally larger differences likely show misclassified water pixels along transition types within stripes.

For turbidity proxy, unaffected lakes showed Landsat 5 values 9% (±18%) higher than Landsat 7, and affected lakes showed a slightly larger difference of 12% (±19%). These changes are consistent with systematic differences between sensors and underestimation of turbid water pixels in interpolated stripes.

Overall, differences between stripe-affected and unaffected lakes are small for both metrics. This indicates that stripe interpolation does not introduce significant systematic bias at the lake scale. While stripes can create uncertainties at the pixel level, their influence at lake scale area and turbidity status metrics is minor, supporting the robustness of the Landsat 7 collection.

Table A1. List of oxbow lakes present in September 2009, indicating SLC-off stripe affectation, differences in water area, and turbidity proxy between the median Landsat 5 TM image and the Landsat 7 ETM+ image.

Name	Stripe-Affected	Water Area			Turbidity Status		
		L5 [km^2]	L7 [km^2]	DWA = (L5 − L7)/L5%	L5%	L7%	DTS = L5 − L7%
OL7	No	2.8	2.8	1.2	96	90	6
OL13	No	1.6	1.6	−1.6	1	3	−2
OL14	No	1.8	1.7	1.1	92	90	2
OL16	No	1.7	1.7	−2.8	54	4	50
OL18	No	1.7	1.7	−0.5	95	94	1
OL19	No	0.3	0.3	0.0	94	94	−1
OL31	No	0.6	0.6	1.1	84	71	13
OL32	No	0.4	0.4	4.9	92	94	−1
OL1	Yes	0.6	0.6	4.9	93	82	12
OL2	Yes	1.3	1.3	5.3	96	80	16
OL3	Yes	0.8	0.8	−0.7	77	1	76
OL4	Yes	0.5	0.5	7.1	35	16	19
OL5	Yes	1.4	1.4	1.2	94	85	9
OL8	Yes	2.4	2.3	1.1	97	94	4
OL10	Yes	1.1	1.1	0.6	95	93	1
OL12	Yes	0.5	0.5	0.0	95	94	1
OL20	Yes	1.8	1.8	2.3	13	32	−20
OL22	Yes	1.1	1.0	6.2	98	93	5
OL25	Yes	1.9	1.9	0.2	85	76	8
OL27	Yes	0.8	0.8	−1.5	96	84	12
OL30	Yes	1.1	1.1	−0.2	89	55	33
OL33	Yes	0.4	0.4	9.6	26	4	22
OL35	Yes	1.8	1.7	6.9	86	80	6
OL37	Yes	1.6	1.6	0.8	98	93	5
OL39	Yes	2.9	2.8	1.0	12	7	5
OL40	Yes	2.5	2.5	0.7	5	0	5

L5: Landsat 5 TM (September 2009 median), L7: Landsat 7 ETM+ (7 September 2009); DWA: Difference in water area %, DTS: Difference in turbidity status %.

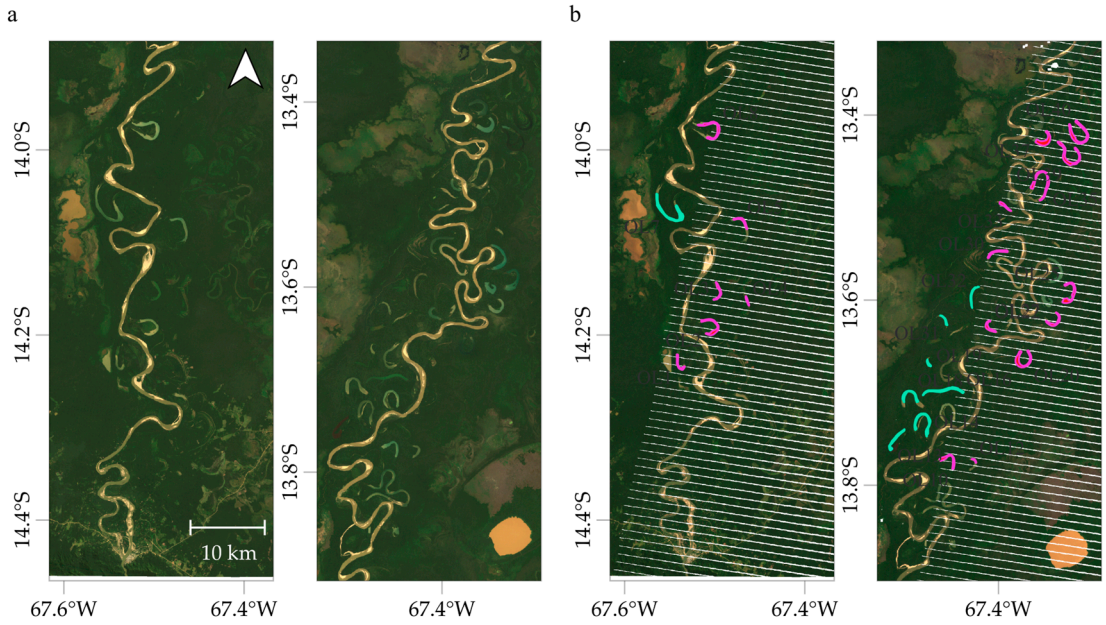

Figure A1. Red, green, blue raw composites of September 2009 imagery used for the SLC-off stripe interpolation evaluation: (**a**) Median Landsat 5 TM image (30 August and 15 September 2009), (**b**) Landsat 7 ETM+ image (7 September 2009) showing oxbow lakes affected (magenta) and unaffected by stripes (cyan).

Table A2. Mean and standard deviation of water area and turbidity proxy differences between Landsat 5 TM (September 2009 median) and Landsat 7 ETM+ (7 September 2009) for stripe-affected and unaffected oxbow lakes.

Group	DWA Mean (SD)	DTS Mean (SD)
Unaffected lakes	0.4 (+/−2.3)	9 (+/−18)
Stripe-affected lakes	2.5 (+/−3.2)	12 (+/−19)

DWA: Difference in water area %, DTS: Difference in turbidity status %; SD: Standard deviation.

Appendix B

The water types defined in Table 1 of the main document were derived from the analysis of the 4 April 2022 Landsat image, which was also used as the training dataset for the random forest classifier. This image represents a transitional hydrologic period in which oxbow lakes show a wide range of connectivity levels and, consequently, a broad range of water conditions. Reflectance values were extracted only from valid unmasked pixels. As shown in Figure A2, the April 2022 scene contains a more complete combination of clear and turbid water types in the oxbow lakes than those typically present during extreme dry or fully flooded periods.

To verify that the spectral variability captured in the April 2022 image is representative of the variability observed during extreme hydrologic conditions (dry on 10 September 2016 and flooded on 11 January 2021), the mean surface reflectance of 30 oxbow lakes was calculated. These lakes have been present since 2015 and have not been eroded by the main channel until 2021. Figure A3 illustrates the mean spectral reflectance for each lake and hydrologic condition, while Figure A4 summarizes this information using boxplots for each spectral band. Together, these figures show that the image of 4 April 2022 includes most of the spectral variation observed in the extreme hydrologic conditions, supporting its suitability for defining water types and training the classifier. The different connectivity

levels of the oxbow lakes during transitional periods extend the diversity of spectral signatures as observed in this image.

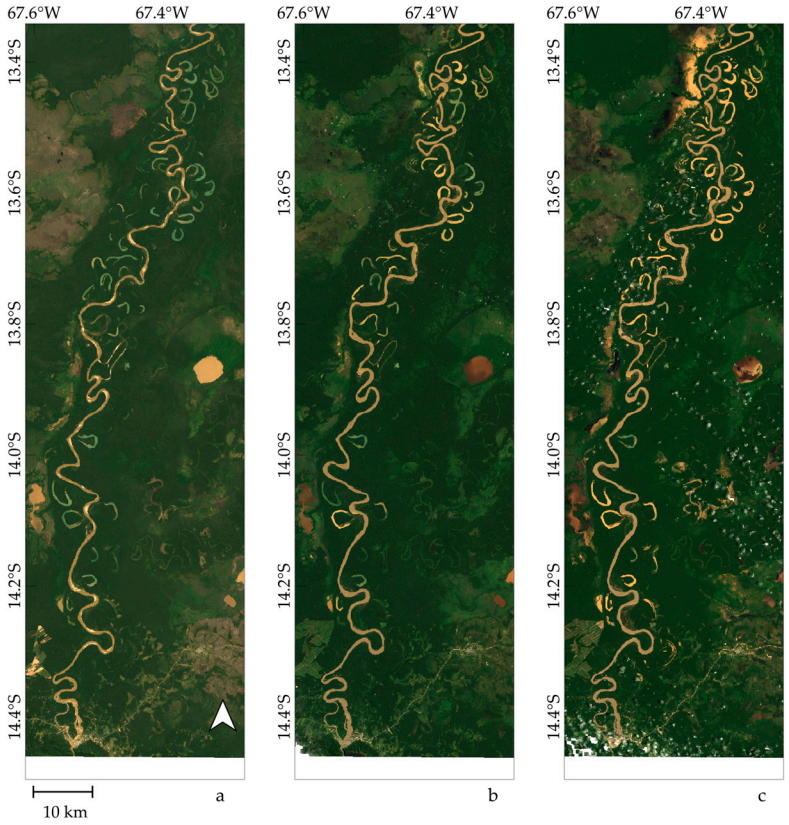

Figure A2. Preprocessed red–green–blue (RGB) composites of Landsat 7 ETM+ images representing three hydrologic conditions in the study area: (**a**) dry period (10 September 2016), (**b**) transitional/normal conditions (4 April 2022), and (**c**) flooded period (11 January 2021).

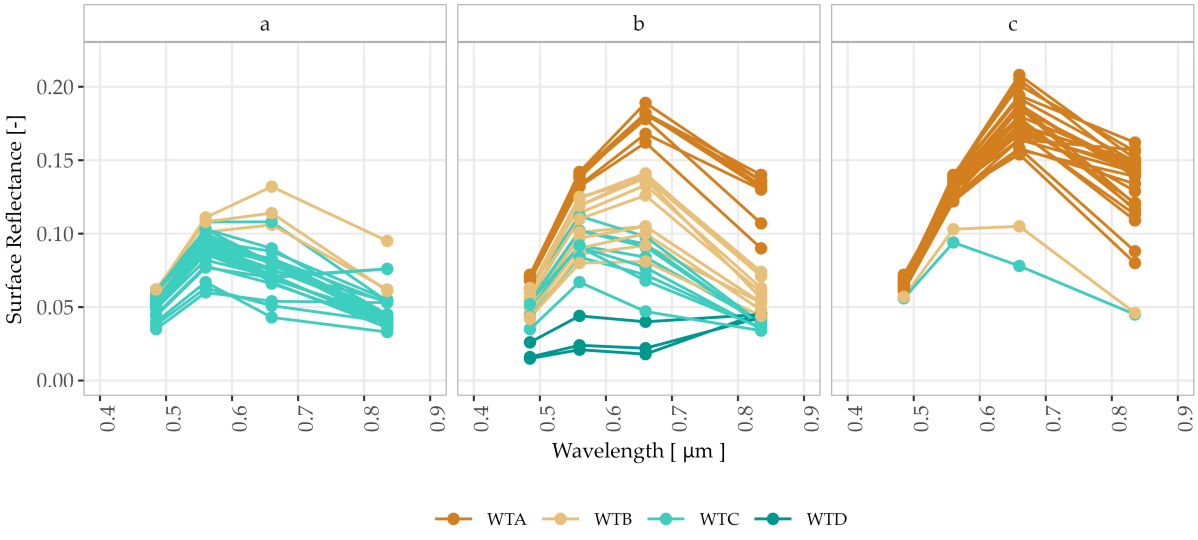

Figure A3. Mean surface reflectance (points mark blue, green, red, and near-infrared bands) for 30 oxbow lakes under three hydrologic conditions: (**a**) dry (10 September 2016), (**b**) transitional/normal (4 April 2022), and (**c**) flooded (11 January 2021).

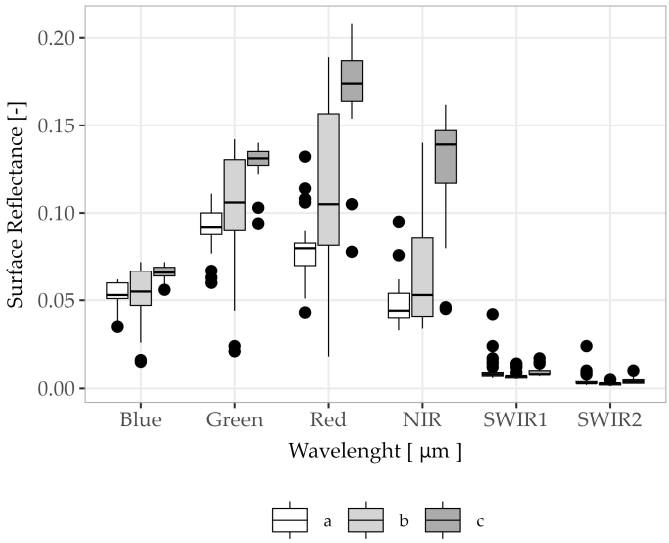

Figure A4. Boxplots of mean surface reflectance for the blue, green, red, near-infrared (NIR), shortwave infrared 1 (SWIR1), and SWIR2 bands for 30 oxbow lakes under three hydrologic conditions: (a) dry (10 September 2016), (b) transitional/normal (4 April 2022), and (c) flooded (11 January 2021).

Appendix C

Table A3. Lake properties.

Lake	Year o (*)	Altered	Age	Distance	Recent Area [km^2]	Turbidity Category	AAT (+)	Low TS (~)	Low TS Dur. (^)	High TS (!)	MAV (#)	QPC	WPC
OL1	1999	NA	Old	Medium	0.69	Turbid	Increase	July	1	August	Medium	$0.61^{1}, 1 \times 10^{-9}, 84$	0.5
OL2	1999	NA	Old	Medium	1.64	Intermediate	Decrease	May	3	August	Low	$0.48^{1}, 2 \times 10^{-5}, 73$	0.7
OL3	1999	NA	Old	Medium	0.81	Clear	Constant	April	9	N	Low	$-0.09^{3}, 4 \times 10^{-1}, 71$	0.9
OL4	1999	NA	Old	Far	0.63	Clear	Mixed	April	10	N	Medium	$-0.07^{3}, 5 \times 10^{-1}, 91$	0.9
OL5	1999	NA	Old	Medium	1.34	Intermediate	Decrease	May	3	August	Low	$0.06^{3}, 6 \times 10^{-1}, 86$	0.8
OL6	2013	NA	Middle	Close	2.19	Turbid	Decrease	July	1	August	High	$0.67^{1}, 2 \times 10^{-4}, 26$	-
OL7	1999	NA	Old	Medium	2.66	Intermediate	Constant	April	4	August	Low	$0.10^{3}, 3 \times 10^{-1}, 91$	0.8
OL8	2005	NA	Middle	Medium	2.28	Intermediate	Decrease	April	4	August	Low	$0.08^{3}, 5 \times 10^{-1}, 73$	0.8
OL9	2016	NA	Recent	Close	1.30	Intermediate	Mixed	June	2	August	High	$0.62^{1}, 1 \times 10^{-2}, 15$	-
OL10	1999	NA	Old	Close	1.10	Intermediate	Constant	April	5	September	Low	$0.20^{2}, 5 \times 10^{-2}, 96$	0.7
OL11	2017	NA	Recent	Medium	0.67	Turbid	Constant	April	1	May	Low	$0.47^{1}, 5 \times 10^{-2}, 18$	-
OL12	1999	NA	Old	Far	0.41	Intermediate	Decrease	April	4	August	Medium	$0.17^{2}, 1 \times 10^{-1}, 94$	0.9
OL13	1999	NA	Old	Medium	1.39	Clear	Decrease	April	9	N	Low	$-0.16^{3}, 1 \times 10^{-1}, 97$	−0.9
OL14	1999	NA	Old	Medium	1.88	Intermediate	Decrease	April	5	September	Low	$0.18^{2}, 8 \times 10^{-2}, 97$	0.7
OL15	2014	AMC	Recent	Close	0.44	Intermediate	Mixed	June	2	August	Medium	$0.29^{2}, 2 \times 10^{-1}, 22$	-
OL16	1999	NA	Old	Medium	1.65	Intermediate	Increase	May	4	September	Low	$0.03^{3}, 8 \times 10^{-1}, 96$	0.0
OL17	2015	AMC	Recent	Close	0.80	Turbid	Constant	NA	N	N	Low	$0.48^{1}, 7 \times 10^{-2}, 15$	-
OL18	1999	NA	Old	Far	1.61	Turbid	Decrease	April	3	July	Medium	$0.11^{2}, 3 \times 10^{-1}, 94$	0.9
OL19	1999	NA	Old	Far	0.30	Intermediate	Decrease	April	3	July	Low	$0.16^{2}, 1 \times 10^{-1}, 94$	0.9
OL20	1999	NA	Old	Medium	1.72	Clear	Increase	June	4	October	Low	$0.07^{3}, 6 \times 10^{-1}, 64$	0.0
OL21	2020	AMC	Recent	Close	1.77	Turbid	Decrease	June	1	July	Medium	$0.48^{1}, 7 \times 10^{-2}, 15$	NA
OL22	1999	NA	Old	Medium	1.05	Intermediate	Decrease	June	2	August	Medium	$0.21^{2}, 4 \times 10^{-2}, 98$	0.7
OL23	2018	AMC	Recent	Close	0.42	Turbid	Mixed	June	2	August	Medium	$0.34^{2}, 2 \times 10^{-1}, 14$	NA
OL24	2012	NA	Middle	Medium	1.18	Clear	Mixed	April	5	September	Medium	$0.37^{2}, 3 \times 10^{-2}, 36$	0.3
OL25	1999	NA	Old	Medium	1.87	Clear	Constant	April	6	October	Low	$0.08^{3}, 5 \times 10^{-1}, 102$	0.3
OL26	2011	AMC	Middle	Medium	1.68	Intermediate	Constant	June	3	September	Low	$0.11^{2}, 4 \times 10^{-1}, 50$	0.1
OL27	1999	NA	Old	Far	0.76	Clear	Constant	May	5	October	Medium	$0.08^{3}, 4 \times 10^{-1}, 105$	0.7
OL28	2017	NA	Recent	Close	1.17	Turbid	Mixed	June	2	August	High	$0.70^{1}, 8 \times 10^{-3}, 13$	NA

Table A3. *Cont.*

Lake	Year o (*)	Altered	Age	Distance	Recent Area [km^2]	Turbidity Category	AAT (+)	Low TS (~)	Low TS Dur. (^)	High TS (!)	MAV (#)	QPC	WPC
OL29	2018	NA	Recent	Close	1.68	Intermediate	Constant	June	2	August	Low	0.56^{1}, 5×10^{-2}, 13	NA
OL30	1999	NA	Old	Close	1.06	Intermediate	Constant	May	5	October	Low	-0.06^{3}, 5×10^{-1}, 110	−0.1
OL31	1999	NA	Old	Far	0.72	Turbid	Mixed	May	2	July	High	0.43^{1}, 5×10^{-6}, 104	0.9
OL32	1999	NA	Old	Far	0.46	Intermediate	Mixed	April	4	August	High	0.54^{1}, 2×10^{-9}, 108	0.9
OL33	1999	NA	Old	Close	0.70	Turbid	Increase	May	1	June	High	0.66^{1}, 2×10^{-15}, 111	0.8
OL34	2013	AMC	Middle	Close	0.34	Intermediate	Constant	June	2	August	Medium	0.31^{2}, 7×10^{-2}, 36	0.2
OL35	2008	NA	Middle	Medium	2.20	Intermediate	Increase	May	4	September	Medium	0.49^{1}, 2×10^{-4}, 54	−0.2
OL36	2015	NA	Recent	Close	1.82	Intermediate	Increase	April	5	September	Medium	0.25^{2}, 2×10^{-1}, 28	NA
OL37	2003	AMC	Middle	Close	1.59	Clear	Constant	May	5	October	Low	0.05^{3}, 6×10^{-1}, 83	−0.1
OL38	2019	AMC	Recent	Close	1.50	Intermediate	Constant	June	3	September	Low	0.51^{1}, 4×10^{-2}, 16	NA
OL39	1999	NA	Old	Far	2.89	Intermediate	Constant	May	5	October	Low	0.19^{2}, 4×10^{-2}, 114	0.4
OL40	1999	NA	Old	Far	2.52	Clear	Constant	May	8	N	Low	0.10^{3}, 3×10^{-1}, 111	−0.3

(*) Year o: First year of data; AMC: Altered by main channel; NA: Not altered by main channel; (+) AAT: Annual lake area trend; (~) Low TS: Month in which low turbidity status starts more frequently; (^) Low TS Dur.: More frequent duration of low turbidity status in months; (!) High TS: Month in which high turbidity status starts more frequently; N: high turbidity status is not frequent in any month; (#) MAV: Monthly lake area variability; QPC: Pearson correlation between log discharge and area difference with annual mean (%), group number in superscript (1, 2, 3), *p*-value, and sample size; WPC: Pearson correlation between mean monthly turbidity status and wind speed for the period 2010–2016.

Appendix D

Wind influence was further analyzed using a high-resolution image and a quantitative analysis of monthly wind speed.

Figure A5 shows selected oxbow lakes in the high-resolution imagery from 7 November 2020 (Map data: ©2020 Maxar Technologies, Google Earth Pro 7.3.6.10441). Yellow arrows indicate areas where suspended sediment traces originate, typically along inner lake margins where exposed sand bars and low water levels make lakes more sensitive to wind-driven mixing. The effect is most evident in clear water lakes (e.g., OL7 and OL14).

Daily wind speed data from the Rurrenabaque airport station is available for 2010–2016 as recorded by the National Service of Meteorology and Hydrology (SENAMHI). The boxplot in Figure A6 presents the distribution of daily wind speeds aggregated by month, showing high variability, and the mean monthly wind speed that peaks from September to December, coinciding with the transition from the dry period to rising water levels.

Figure A7 shows scatter plots of mean monthly wind speed versus mean monthly turbidity status for lakes with available observations (cloud-free images from April to September). Pearson correlation values (Table A3 and column WPC, Appendix C) show that eleven lakes have correlations above 0.7 (mostly old lakes), while eleven lakes have insufficient data, and the rest show weak correlation.

Overall, both qualitative and quantitative analyses indicate that wind contributes to sediment resuspension in oxbow lakes, likely interacting with the early input of turbid water at the beginning of the flooding period.

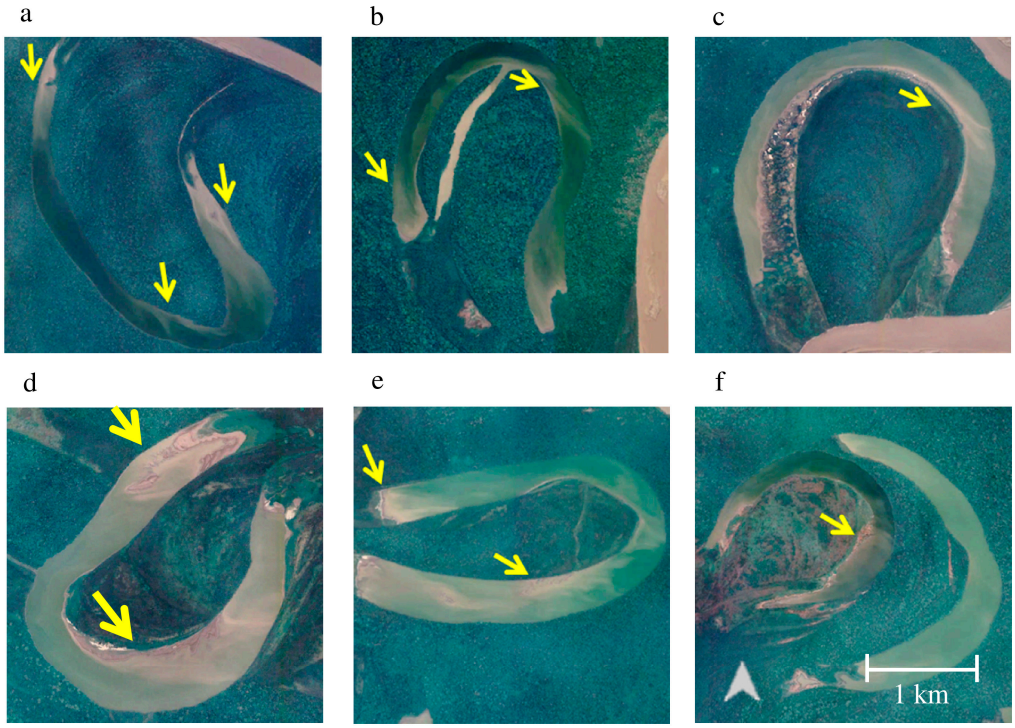

Figure A5. High-resolution Google Earth Pro imagery on 07 November 2020 (©2020 Maxar Technologies) of selected oxbow lakes with wind-driven suspended-sediment traces (origin pointed by yellow arrows): (**a**) OL7, (**b**) OL14, (**c**) OL28, (**d**) OL29, (**e**) OL21, and (**f**) OL24 (inner) and OL26.

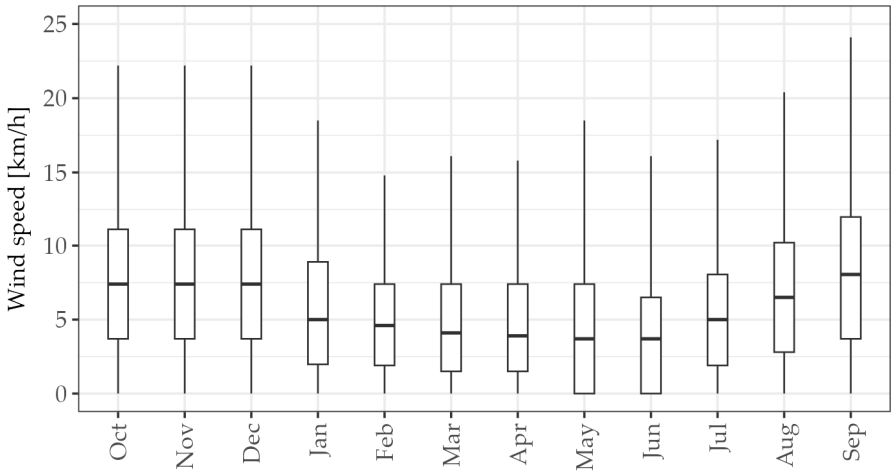

Figure A6. Distribution of daily wind speeds [km/h] aggregated by month and mean monthly wind speed observed at the Rurrenabaque airport station (2010–2016; SENAMHI), indicating higher values from September to December.

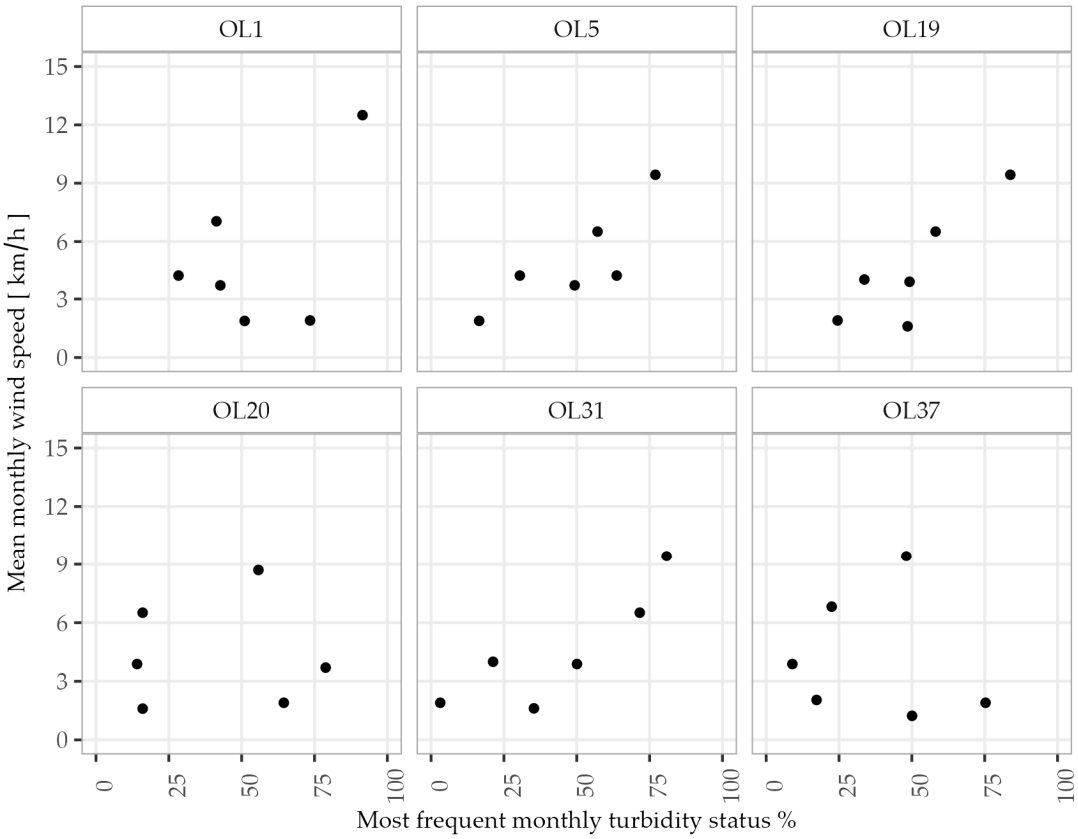

Figure A7. Scatter plots of mean monthly wind speed (2010–2016) vs. most frequent monthly turbidity status (available for cloud-free images from April to September) for selected lakes with high (OL5, OL19, OL31) and low (OL1, OL20, OL37) Pearson correlation.

References

1. Alcântara, E.; Edward, P. Editorial for the Special Issue "Remote Sensing of Large Rivers". *Remote Sens.* **2020**, *12*, 1244. [CrossRef]
2. Park, E.; Latrubesse, E.M. Modeling Suspended Sediment Distribution Patterns of the Amazon River Using MODIS Data. *Remote Sens. Environ.* **2014**, *147*, 232–242. [CrossRef]
3. Rudorff, C.M.; Dunne, T.; Melack, J.M. Recent Increase of River–Floodplain Suspended Sediment Exchange in a Reach of the Lower Amazon River. *Earth Surf. Process. Landf.* **2018**, *43*, 322–332. [CrossRef]

4. Borghezan, E.d.A.; Pires, T.H.d.S.; Ikeda, T.; Zuanon, J.; Kohshima, S. A Review on Fish Sensory Systems and Amazon Water Types with Implications to Biodiversity. *Front. Ecol. Evol.* **2021**, *8*, 589760. [CrossRef]
5. Junk, W.J.; Wittmann, F.; Schöngart, J.; Piedade, M.T.F.; da Cunha, C.N. Large Rivers and Their Floodplains. In *Introducing Large Rivers*; Gupta, A., Slaymaker, O., Junk, W.J., Eds.; John Wiley & Sons Ltd.: Chichester, UK, 2020; pp. 55–101.
6. Junk, W.J.; Bailey, P.B.; Sparks, R.E. The Flood Pulse Concept in River-Floodplain Systems. In *Proceedings of the International Large River Symposium*; Dodge, D.P., Ed.; Department of Fisheries and Oceans: Ottawa, ON, Canada, 1989; Volume 106, pp. 110–127.
7. Gorelick, N.; Hancher, M.; Dixon, M.; Ilyushchenko, S.; Thau, D.; Moore, R. Google Earth Engine: Planetary-Scale Geospatial Analysis for Everyone. *Remote Sens. Environ.* **2017**, *202*, 18–27. [CrossRef]
8. Mutanga, O.; Kumar, L. Google Earth Engine Applications. *Remote Sens.* **2019**, *11*, 591. [CrossRef]
9. Sogno, P.; Klein, I.; Kuenzer, C. Remote Sensing of Surface Water Dynamics in the Context of Global Change—A Review. *Remote Sens.* **2022**, *14*, 2475. [CrossRef]
10. Lewin, J.; Ashworth, P.J. Defining Large River Channel Patterns: Alluvial Exchange and Plurality. *Geomorphology* **2014**, *215*, 83–98. [CrossRef]
11. Herrera-R, G.A.; Heilpern, S.A.; Couto, T.B.A.; Victoria-Lacy, L.; Duponchelle, F.; Correa, S.B.; Farah-Pérez, A.; López-Casas, S.; Cañas-Alva, C.M.; Doria, C.R.C.; et al. A Synthesis of the Diversity of Freshwater Fish Migrations in the Amazon Basin. *Fish Fish.* **2024**, *25*, 114–133. [CrossRef]
12. Melack, J.M.; Novo, E.M.L.M.; Forsberg, B.R.; Piedade, M.T.F.; Maurice, L. Floodplain Ecosystem Processes. In *Amazonia and Global Change*; Keller, M., Bustamante, M., Gash, J., Silva-Dias, P., Eds.; Geophysical Monograph Series; American Geophysical Union: Washington, DC, USA, 2009; Volume 186, pp. 525–541, ISBN 978-0-87590-476-4.
13. Welcomme, R.L. *River Fisheries*; FAO Fisheries Technical Paper; FAO: Rome, Italy, 1985; ISBN 92-5-102299-2.
14. Isaac, V.J.; Castello, L.; Santos, P.R.B.; Ruffino, M.L. Seasonal and Interannual Dynamics of River-Floodplain Multispecies Fisheries in Relation to Flood Pulses in the Lower Amazon. *Fish. Res.* **2016**, *183*, 352–359. [CrossRef]
15. Santos, R.E.; Pinto-Coelho, R.M.; Drumond, M.A.; Fonseca, R.; Zanchi, F.B. Damming Amazon Rivers: Environmental Impacts of Hydroelectric Dams on Brazil's Madeira River According to Local Fishers' Perception. *Ambio* **2020**, *49*, 1612–1628. [CrossRef]
16. Lauzanne, L.; Loubens, G.; Le Guennec, B. Pesca y Biología Pesquera En El Mamoré Médio (Región de Trinidad, Bolívia). *Interciencia* **1990**, *15*, 452–460.
17. Santos, R.E.; Pinto-Coelho, R.M.; Fonseca, R.; Simões, N.R.; Zanchi, F.B. The Decline of Fisheries on the Madeira River, Brazil: The High Cost of the Hydroelectric Dams in the Amazon Basin. *Fish. Manag. Ecol.* **2018**, *25*, 380–391. [CrossRef]
18. Crosato, A. *Analysis and Modelling of River Meandering*; IOS Press: Amsterdam, The Netherlands, 2008; ISBN 978-1-58603-915-8.
19. Hooke, J.M. River Meandering. In *Treatise on Geomorphology*; Shroder, J., Ed.; Academic Press: Oxford, UK, 2013; Volume 9, pp. 480–516, ISBN 978-0-12-818235-2.
20. Dunne, T.; Aalto, R. Large River Floodplains. In *Treatise on Geomorphology*; Shroder, J., Ed.; Academic Press: Oxford, UK, 2013; Volume 9, pp. 645–678, ISBN 978-0-08-088522-3.
21. Saucier, R.T. *Geomorphology and Quaternary Geologic History of the Lower Mississippi Valley*; U.S. Army Corps of Engineer Waterways Experiment Station: Vicksburg, MS, USA, 1994; Volume 1, ISBN 39180-6199.
22. Wren, D.G.; Davidson, G.R.; Walker, W.G.; Galicki, S.J. The Evolution of an Oxbow Lake in the Mississippi Alluvial Floodplain. *J. Soil Water Conserv.* **2008**, *63*, 129–135. [CrossRef]
23. Gautier, E.; Brunstein, D.; Vauchel, P.; Jouanneau, J.M.; Roulet, M.; Garcia, C.; Guyot, J.L.; Castro, M. Channel and Floodplain Sediment Dynamics in a Reach of the Tropical Meandering Rio Beni (Bolivian Amazonia). *Earth Surf. Process. Landf.* **2010**, *35*, 1838–1853. [CrossRef]
24. Hudson, P.F.; Heitmuller, F.T.; Leitch, M.B. Hydrologic Connectivity of Oxbow Lakes along the Lower Guadalupe River, Texas: The Influence of Geomorphic and Climatic Controls on the "Flood Pulse Concept". *J. Hydrol.* **2012**, *414–415*, 174–183. [CrossRef]
25. Paulino, R.S.; Martins, V.S.; Novo, E.M.L.d.M.; Maciel, D.A.; Correia-Lima, D.L.; Barbosa, C.C.F.; Bonnet, M.P.; Uhde, A. A Framework Based on Spectral Similarity to Estimate Hydrological Connectivity in Juruá River Floodplain Lakes Using 3-m PlanetScope Data. *J. Hydrol.* **2023**, *625*, 130156. [CrossRef]
26. Tejerina-Garro, F.L.; Fortin, R.; Rodríguez, M.A. Fish Community Structure in Relation to Environmental Variation in Floodplain Lakes of the Araguaia River, Amazon Basin. *Environ. Biol. Fishes* **1998**, *51*, 399–410. [CrossRef]
27. Santana, A.R.A.; Werth, M.; Benedito, E. Use of Food Resources by Detritivorous Fish in Floodplains: A Synthesis. *Acta Biológica Colomb.* **2015**, *20*, 5–14. [CrossRef]
28. Maurice-Bourgoin, L.; Bonnet, M.P.; Martinez, J.M.; Kosuth, P.; Cochonneau, G.; Moreira-Turcq, P.; Guyot, J.L.; Vauchel, P.; Filizola, N.; Seyler, P. Temporal Dynamics of Water and Sediment Exchanges between the Curuaí Floodplain and the Amazon River, Brazil. *J. Hydrol.* **2007**, *335*, 140–156. [CrossRef]
29. Gholizadeh, M.H.; Melesse, A.M.; Reddi, L. A Comprehensive Review on Water Quality Parameters Estimation Using Remote Sensing Techniques. *Sensors* **2016**, *16*, 1298. [CrossRef]

30. Spyrakos, E.; O'Donnell, R.; Hunter, P.D.; Miller, C.; Scott, M.; Simis, S.G.H.; Neil, C.; Barbosa, C.C.F.; Binding, C.E.; Bradt, S.; et al. Optical Types of Inland and Coastal Waters. *Limnol. Oceanogr.* **2018**, *63*, 846–870. [CrossRef]
31. da Silva, E.F.F.; Novo, E.M.L.d.M.; Lobo, F.d.L.; Barbosa, C.C.F.; Noernberg, M.A.; Rotta, L.H.d.S.; Tressmann, C.C.; Maciel, D.A.; Flores, R.J. Optical Water Types Found in Brazilian Waters. *Limnology* **2021**, *22*, 57–68. [CrossRef]
32. Martinez, J.M.; Espinoza-Villar, R.; Armijos, E.; Silva-Moreira, L. The Optical Properties of River and Floodplain Waters in the Amazon River Basin: Implications for Satellite-Based Measurements of Suspended Particulate Matter. *J. Geophys. Res. Earth Surf.* **2015**, *120*, 1274–1287. [CrossRef]
33. Valerio, A.d.M.; Kampel, M.; Vantrepotte, V.; Ward, N.D.; Richey, J.E. Optical Classification of Lower Amazon Waters Based on In Situ Data and Sentinel-3 Ocean and Land Color Instrument Imagery. *Remote Sens.* **2021**, *13*, 3057. [CrossRef]
34. Barbosa, C.C.F. Metodologia de Análise Da Dinâmica de Área e Volume Inundável: O Exemplo Da Várzea Do Lago Grande de Curuaí. *Rev. Bras. Cartogr.* **2006**, *58*, 201–210. Available online: http://urlib.net/rep/sid.inpe.br/ePrint@80/2006/03.23.20.06 (accessed on 1 July 2024). [CrossRef]
35. Fassoni-Andrade, A.C.; Paiva, R.C.D. de Mapping Spatial-Temporal Sediment Dynamics of River-Floodplains in the Amazon. *Remote Sens. Environ.* **2019**, *221*, 94–107. [CrossRef]
36. da Silva, E.F.F.; Novo, E.M.L.d.M.; Lobo, F.d.L.; Barbosa, C.C.F.; Tressmann, C.C.; Noernberg, M.A.; Rotta, L.H.d.S. A Machine Learning Approach for Monitoring Brazilian Optical Water Types Using Sentinel-2 MSI. *Remote Sens. Appl. Soc. Environ.* **2021**, *23*, 100577. [CrossRef]
37. Maciel, D.A.; Barbosa, C.C.F.; Novo, E.M.L.d.M.; Flores, R.J.; Begliomini, F.N. Water Clarity in Brazilian Water Assessed Using Sentinel-2 and Machine Learning Methods. *ISPRS J. Photogramm. Remote Sens.* **2021**, *182*, 134–152. [CrossRef]
38. Aggarwal, C.C. *Data Mining The Text Book*; Springer: Yorktown Heights, NY, USA, 2015; ISBN 978-3-319-14141-1.
39. Breiman, L. Random Forests. *Mach. Learn.* **2001**, *45*, 5–32. [CrossRef]
40. Safavian, S.R.; Landgrebe, D. A Survey of Decision Tree Classifier Methodology. *IEEE Trans. Syst. Man Cybern.* **1991**, *21*, 660–674. [CrossRef]
41. Terborgh, J.W.; Davenport, L.C.; Belcon, A.U.; Katul, G.; Swenson, J.J.; Fritz, S.C.; Baker, P.A. Twenty-Three-Year Timeline of Ecological Stable States and Regime Shifts in Upper Amazon Oxbow Lakes. *Hydrobiologia* **2018**, *807*, 99–111. [CrossRef]
42. Ahmed, J. Establishing the Hydrological Controls on Water Surface Area Variations in Oxbow Lakes. *Hydrol. Process.* **2024**, *38*, e70013. [CrossRef]
43. Wang, D.; Li, Z.; Li, Z.; Pan, B.; Tian, S.; Nie, X. Environmental Gradient Relative to Oxbow Lake-Meandering River Connectivity in Zoige Basin of the Tibetan Plateau. *Ecol. Eng.* **2020**, *156*, 105983. [CrossRef]
44. Terrazas-Villarroel, L.G.; Wenninger, J.; Heredia-Gómez, M.; van de Giesen, N.; McClain, M.E. Exploring Ecohydrology Through the Lens of Local Fishers in the Bolivian Amazon. *Ecosphere* **2026**, *in press*.
45. Espinoza, J.C.; Garreaud, R.; Poveda, G.; Arias, P.A.; Molina-Carpio, J.; Masiokas, M.; Viale, M.; Scaff, L. Hydroclimate of the Andes Part I: Main Climatic Features. *Front. Earth Sci.* **2020**, *8*, 64. [CrossRef]
46. Molina-Carpio, J.; Espinoza, J.C.; Vauchel, P.; Ronchail, J.; Gutierrez-Caloir, B.; Guyot, J.; Noriega, L. Hydroclimatology of the Upper Madeira River Basin: Spatio-Temporal Variability and Trends. *Hydrol. Sci. J.* **2017**, *62*, 911–927. [CrossRef]
47. Vauchel, P.; Santini, W.; Guyot, J.L.; Moquet, J.S.; Martinez, J.M.; Espinoza, J.C.; Baby, P.; Fuertes, O.; Noriega, L.; Puita, O.; et al. A Reassessment of the Suspended Sediment Load in the Madeira River Basin from the Andes of Peru and Bolivia to the Amazon River in Brazil, Based on 10 Years of Data from the HYBAM Monitoring Programme. *J. Hydrol.* **2017**, *553*, 35–48. [CrossRef]
48. Constantine, J.A.; Dunne, T.; Ahmed, J.; Legleiter, C.; Lazarus, E.D. Sediment Supply as a Driver of River Meandering and Floodplain Evolution in the Amazon Basin. *Nat. Geosci.* **2014**, *7*, 899–903. [CrossRef]
49. Schwendel, A.C.; Nicholas, A.P.; Aalto, R.E.; Sambrook-Smith, G.H.; Buckley, S. Interaction between Meander Dynamics and Floodplain Heterogeneity in a Large Tropical Sand-Bed River: The Rio Beni, Bolivian Amazon. *Earth Surf. Process. Landf.* **2015**, *40*, 2026–2040. [CrossRef]
50. Gautier, E.; Brunstein, D.; Vauchel, P.; Roulet, M.; Fuertes, O.; Guyot, J.L.; Darozzes, J.; Bourrel, L. Temporal Relations between Meander Deformation, Water Discharge and Sediment Fluxes in the Floodplain of the Rio Beni (Bolivian Amazonia). *Earth Surf. Process. Landf.* **2007**, *32*, 230–248. [CrossRef]
51. Schmidt, G.; Jenkerson, C.B.; Masek, J.; Vermote, E.; Gao, F. *Landsat Ecosystem Disturbance Adaptive Processing System (LEDAPS) Algorithm Description*; U.S. Geological Survey: Reston, VA, USA, 2013; ISBN 2331-1258.
52. Chávez-Flores, I.A. Análisis, Crítica y Relleno de Las Series Continuas Hidrológicas de la Amazonia Boliviana. Bachelor's Thesis, Universidad Mayor de San Simón, Cochabamba, Bolivia, 2020.
53. Rouse, J.W.; Haas, R.H.; Schell, J.A.; Deering, D.W. Monitoring Vegetation Systems in the Great Plains with ERTS. In *Proceedings of the Third Earth Resources Technology Satellite-1 Symposium, Technical Presentations*; NASA Goddard Space Flight Center: Washington, DC, USA, 1974; Volume 1.

54. Berveglieri, A.; Imai, N.N.; Christovam, L.E.; Galo, M.L.B.T.; Tommaselli, A.M.G.; Honkavaara, E. Analysis of Trends and Changes in the Successional Trajectories of Tropical Forest Using the Landsat NDVI Time Series. *Remote Sens. Appl. Soc. Environ.* **2021**, *24*, 100622. [CrossRef]
55. Secu, C.V.; Stoleriu, C.C.; Lesenciuc, C.D.; Ursu, A. Normalized Sand Index for Identification of Bare Sand Areas in Temperate Climates Using Landsat Images, Application to the South of Romania. *Remote Sens.* **2022**, *14*, 3802. [CrossRef]
56. Ha, N.T.T.; Thao, N.T.P.; Koike, K.; Nhuan, M.T. Selecting the Best Band Ratio to Estimate Chlorophyll-a Concentration in a Tropical Freshwater Lake Using Sentinel 2A Images from a Case Study of Lake Ba Be (Northern Vietnam). *ISPRS Int. J. Geo-Inf.* **2017**, *6*, 290. [CrossRef]
57. Kirk, J.T.O. *Light and Photosynthesis in Aquatic Ecosystems*, 3rd ed.; Cambridge University Press: Cambridge, UK, 2011; ISBN 978-0-521-15175-7.
58. Moore, T.S.; Dowell, M.D.; Bradt, S.; Ruiz-Verdu, A. An Optical Water Type Framework for Selecting and Blending Retrievals from Bio-Optical Algorithms in Lakes and Coastal Waters. *Remote Sens. Environ.* **2014**, *143*, 97–111. [CrossRef] [PubMed]
59. Montanher, O.C.; Novo, E.M.L.d.M.; Barbosa, C.C.F.; Rennó, C.D.; Silva, T.S.F. Empirical Models for Estimating the Suspended Sediment Concentration in Amazonian White Water Rivers Using Landsat 5/TM. *Int. J. Appl. Earth Obs. Geoinf.* **2014**, *29*, 67–77. [CrossRef]
60. Bhargava, D.S.; Mariam, D.W. Effects of Suspended Particle Size and Concentration on Reflectance Measurements. *Photogramm. Eng. Remote Sens.* **1991**, *57*, 519–529. Available online: http://pascal-francis.inist.fr/vibad/index.php?action=getRecordDetail&idt=19664986 (accessed on 1 December 2024).
61. Kwon, S.; Noh, H.; Seo, I.W.; Park, Y.S. Effects of Spectral Variability Due to Sediment and Bottom Characteristics on Remote Sensing for Suspended Sediment in Shallow Rivers. *Sci. Total Environ.* **2023**, *878*, 163125. [CrossRef]
62. Novo, E.M.d.M.; Hansom, J.D.; Curran, P.J. The Effect of Sediment Type on the Relationship between Reflectance and Suspended Sediment Concentration. *Int. J. Remote Sens.* **1989**, *10*, 1283–1289. [CrossRef]
63. Zhang, Y.; Duan, H.; Xi, H.; Huang, Z.; Tsou, J.; Jiang, T.; Liang, X.S. Evaluation of the Influence of Aquatic Plants and Lake Bottom on the Remote-Sensing Reflectance of Optically Shallow Waters. *Atmosphere-Ocean* **2018**, *56*, 277–288. [CrossRef]
64. Güntzel, A.M.; da Silva, W.M.; Panarelli, E.A. Connectivity as the Control Key to Intensity of Flood Pulse in Taquari River Oxbow Lakes. *Rev. Ambient. Água* **2020**, *15*, e2534. [CrossRef]
65. Toonen, W.H.J.; Kleinhans, M.G.; Cohen, K.M. Sedimentary Architecture of Abandoned Channel Fills. *Earth Surf. Process. Landf.* **2012**, *37*, 459–472. [CrossRef]
66. Citterio, A.; Piégay, H. Overbank Sedimentation Rates in Former Channel Lakes: Characterization and Control Factors. *Sedimentology* **2009**, *56*, 461–482. [CrossRef]
67. Schwendel, A.; Aalto, R.; Nicholas, A.; Parsons, D. Fill Characteristics of Abandoned Channels and Resulting Stratigraphy of a Mobile Sand-bed River Floodplain. In *Fluvial Meanders and Their Sedimentary Products in the Rock Record*; Ghinassi, M., Colombera, L., Mountney, N.P., Reesink, A.J.H., Bateman, M., Eds.; Wiley Blackwell and International Association of Sedimentologists: Oxford, UK, 2018; Volume 48, pp. 251–272.
68. Mertes, L.A.K. Documentation and Significance of the Perirheic Zone on Inundated Floodplains. *Water Resour. Res.* **1997**, *33*, 1749–1762. [CrossRef]
69. Chowdhury, M.A.K.; Yakupitiyage, A. Efficiency of Oxbow Lake Management Systems in Bangladesh to Introduce Cage Culture for Resource-Poor Fisheries. *Fish. Manag. Ecol.* **2000**, *7*, 65–74. [CrossRef]
70. Goetz, D.; Miranda, L.E.; Kröger, R.; Andrews, C. The Role of Depth in Regulating Water Quality and Fish Assemblages in Oxbow Lakes. *Env. Biol Fish* **2015**, *98*, 951–959. [CrossRef]
71. Miranda, L.E. Fish Assemblages in Oxbow Lakes Relative to Connectivity with the Mississippi River. *Trans. Am. Fish. Soc.* **2005**, *134*, 1480–1489. [CrossRef]
72. Osorio, D.; Terborgh, J.; Alvarez, A.; Ortega, H.; Quispe, R.; Chipollini, V.; Davenport, L.C. Lateral Migration of Fish between an Oxbow Lake and an Amazonian Headwater River. *Ecol. Freshw. Fish* **2011**, *20*, 619–627. [CrossRef]
73. Virgilio, L.R.; Silva, A.L.C.; Saldanha, R.F.; Suçuarana, M.d.S.; Fernandes, E.C.; Vieira, L.J.S. Fish Fauna in Oxbow Lakes of the Middle Purus River in the Neotropical Region of the Amazon Rainforest / Fauna de Peixes Em Lagos de Meandro Abandonado No Médio Rio Purus Na Região Amazônica Neotropical. *Braz. J. Dev.* **2020**, *6*, 55545–55564. [CrossRef]

Disclaimer/Publisher's Note: The statements, opinions and data contained in all publications are solely those of the individual author(s) and contributor(s) and not of MDPI and/or the editor(s). MDPI and/or the editor(s) disclaim responsibility for any injury to people or property resulting from any ideas, methods, instructions or products referred to in the content.